

Improving quantum parameter estimation by monitoring quantum trajectoriesYao Ma,¹ Mi Pang,¹ Libo Chen,² and Wen Yang^{3,*}¹*Department of Applied Physics, School of Sciences, Xi'an University of Technology, Xi'an 710048, China*²*School of Science, Qingdao University of Technology, Qingdao 266033, China*³*Beijing Computational Science Research Center, Beijing 100193, China*

(Received 13 January 2019; published 28 March 2019)

Quantum-enhanced parameter estimation has widespread applications in many fields. An important issue is to protect the estimation precision against the noise-induced decoherence. Here we develop a general theoretical framework for improving the precision for estimating an arbitrary parameter by monitoring the noise-induced quantum trajectories (MQT) and establish its connections to the purification-based approach to quantum parameter estimation. Monitoring the noise-induced quantum trajectory can be achieved in two ways: (i) Any quantum trajectories can be monitored by directly monitoring the environment, which is experimentally challenging for realistic noises, and (ii) certain quantum trajectories can also be monitored by frequently measuring the quantum probe alone via ancilla-assisted encoding and error detection. This establishes an interesting connection between MQT and the full quantum-error-correction protocol. Application of MQT to estimate the level splitting and decoherence rate of a spin 1/2 under typical decoherence channels demonstrate that it can avoid the long-time exponential loss of the estimation precision and, in special cases, recover the Heisenberg scaling.

DOI: [10.1103/PhysRevA.99.032347](https://doi.org/10.1103/PhysRevA.99.032347)**I. INTRODUCTION**

The precise estimation of parameters characterizing physical processes [1,2] has applications in many fields, such as gravitational-wave detection [3,4], frequency spectroscopy [5,6], magnetometry [7,8], optical phase estimation [9], and atomic clocks [10]. With classical probes, repeated measurements can be used to improve the estimation precision according to the classical $1/\sqrt{N}$ scaling with respect to the number N of repetitions. With quantum probes, quantum resources (such as entanglement) can be utilized to improve the estimation beyond the classical scaling and even attain the fundamental Heisenberg $1/N$ scaling allowed by quantum mechanics, where N is the number of probes used in the estimation. However, the inevitable presence of environmental noises decoheres the quantum probes [11], limits the available quantum resources, and severely degrades the estimation precision. This poses a critical challenge to the practical realization of quantum-enhanced parameter estimation.

To address this problem, several methods have been developed, such as dynamical decoupling [12–16] (see Refs. [2,17] for a review), time optimization [18–20], and quantum error correction (QEC) [21–28] or feedback control [29–31]. The idea of dynamical decoupling is to apply pulsed [13,16,32–39] or continuous [15,40–42] control on the quantum probe to reduce its coupling to the noise and hence prolong its coherence time. It has achieved remarkable success in detecting alternating signals [43,44], noises [40,41,45–49], and other quantum objects [50–56], but it is only applicable to

non-Markovian noises [57–60]. The idea of time optimization is to mitigate decoherence by shortening the evolution time of the quantum probe. It can improve the scaling of the estimation precision beyond the classical scaling, but requires vanishingly short evolution time and large-scale entanglement. Note that many Markovian environments only allow the classical $1/\sqrt{N}$ scaling even if the most general scheme is employed [61–69]. In this case, using short-range correlated states, which can be modeled by matrix product states [65], already gives almost optimal performance. The idea of QEC is to detect and then correct the noise-induced erroneous evolution. This is a powerful method applicable to both Markovian and non-Markovian noises [21–28]. For Hamiltonian parameter estimation, recent works [68,69] show that when the unitary Hamiltonian evolution can be distinguished from the noise-induced evolution, QEC can even recover the ultimate Heisenberg scaling; otherwise only a constant-factor improvement over the classical scaling is possible.

Very recently, an interesting method was proposed [70–72] to improve the estimation precision. The idea is to monitor the environment [73–75] continuously to (fully or partially) extract the information that leaks into the environment. For certain Markovian environments, this method can recover the Heisenberg scaling [70–72], but previous studies focus on specific Markovian environments and measurements and usually rely on Gaussian approximation or numerically solving the stochastic master equations. Moreover, this method requires direct measurement of the environment, which is very challenging for realistic noise processes.

In this work we address the above problems. First, we develop a general theoretical framework for improving the precision of parameter estimation via continuous monitoring

*wenyang@csrc.ac.cn

of a general (either Markovian or non-Markovian) environment and further establish its connection to the Purification-based approach to quantum parameter estimation [61], which has motivated many works that derive fundamental bounds on the estimation precision [20,62–69,76,77]. Second, for a Markovian environment, we provide a superoperator approach to determine the fundamental bounds on the estimation precision. This approach corresponds to an exact integration of the stochastic master equation [71,72] and may provide exact analytical expressions for some simple models. Third, we relax the conceptually simple but experimentally challenging requirement of monitoring the environment to the concept of monitoring the quantum trajectories (MQT): Any quantum trajectories can be monitored by monitoring the environment, but *certain* quantum trajectories can also be monitored by frequently measuring the quantum probe (without monitoring the environment) via ancilla-assisted encoding and error detection [21–23], i.e., the first two steps of QEC. This QEC-based MQT not only makes certain MQT experimentally feasible, but also establishes an interesting connection between MQT and the full QEC-based metrology [21–28]. The QEC-based MQT can be regarded as a QEC protocol without corrective operations, so it is less powerful than QEC when perfect error correction is available. Nevertheless, MQT itself provides insight into how the information leaks into the distinct quantum trajectories and how it is recovered. Moreover, for certain models where corrective operations are not necessary, the MQT becomes advantageous because it avoids faulty corrective operations that may degrade the estimation precision significantly [22]. We apply this method to the estimation of the level splitting ω and the decoherence rate γ of a spin 1/2 under three decoherence channels: spin relaxation, spin flip, and spin dephasing. We find that it can significantly improve the precision for estimating ω under the spin-relaxation channel, avoid the exponential loss of the precision for estimating γ (estimating ω) under all the decoherence channels (under the spin-flip channel), and even recover the Heisenberg scaling for estimating ω under the spin-dephasing channel.

Monitoring quantum trajectories can be achieved either by directly monitoring the environment or, for certain quantum trajectories, by the first two steps of QEC, i.e., QEC-based MQT. The former can be illustrated for some toy models (e.g., the flip of a spin 1/2 due to its Heisenberg-type exchange interaction with another spin 1/2, which plays the role of the environment, can be detected by measuring the latter), but becomes very challenging for realistic noises, even for very simple cases (e.g., the relaxation of a qubit inside a single-mode cavity is accompanied by the emission of a cavity photon, so detecting the qubit relaxation requires detecting the cavity output at the single-photon level [78–80]). By contrast, QEC-based MQT amounts to quantum error detection without correction (see Sec. II E for a detailed discussion), so it can be achieved in *any* experimental platform where QEC has been demonstrated, such as the nitrogen-vacancy center [26,81,82], superconducting qubits [83,84], and trapped ions [85–87].

This paper is organized as follows. In Sec. II we give the general theory of MQT. In Sec. III we apply MQT to estimate the level splitting and decoherence rate of a spin 1/2. In Sec. IV we summarize and provide conclusions.

II. GENERAL IDEA AND THEORY

To estimate an unknown parameter θ , the quantum probe starts from certain initial state ρ_0 and then undergoes certain θ -dependent evolution for an interval T into the final state $\rho(\theta)$, followed by an optimal measurement of $\rho(\theta)$ to transfer all the information about θ from the quantum probe into the measurement outcome. After repeating the above procedures $\nu \gg 1$ times, we can use the ν measurement outcomes to construct an optimal unbiased estimator to θ , such as the maximum likelihood estimator or the Bayesian estimator [88]. The estimation precision for θ is determined by the quantum Cramér-Rao bound [89,90] as

$$\delta\theta \equiv \frac{1}{\sqrt{\nu\mathcal{F}[\rho(\theta)]}}, \quad (1)$$

where $\mathcal{F}[\rho(\theta)]$ is the quantum Fisher information (QFI) [90] about θ provided by a single copy of $\rho(\theta)$, while $\nu\mathcal{F}[\rho(\theta)]$ is the total QFI provided by ν copies of $\rho(\theta)$. In Appendix A we provide a detailed introduction to all the relevant concepts, such as QFI, classical Fisher information (CFI), optimal measurements, and optimal unbiased estimators.

A. Nonunitary evolution and purification

When the environment (or the quantum trajectories of the quantum probe) is not monitored, the noise-induced decoherence during the θ -dependent evolution is a black box [see Fig. 1(a)], so our state of knowledge about the quantum probe is described by the nonselective density matrix $\bar{\rho}(t)$. The most general nonunitary evolution of $\bar{\rho}(t)$ is described by a time-local master equation [91,92]

$$\frac{d}{dt}\bar{\rho}(t) = \mathcal{L}(t)\bar{\rho}(t),$$

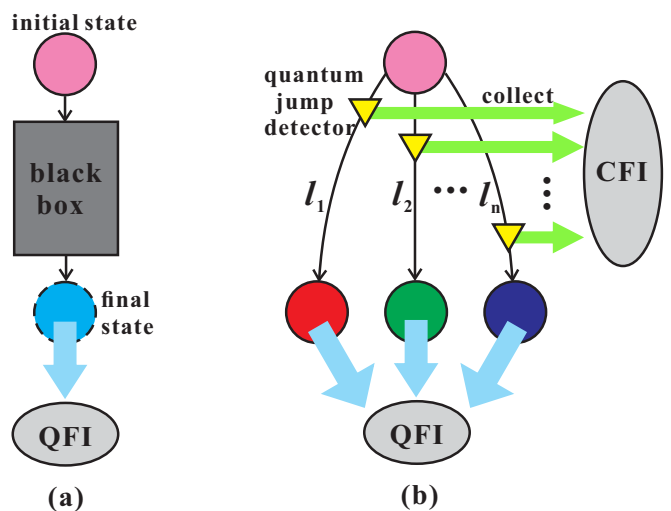


FIG. 1. Quantum parameter estimation by (a) conventional method and (b) monitoring quantum trajectories: The former treats the noise-induced decoherence as a black box, while the latter gains access to the quantum Fisher information of every trajectory and the classical Fisher information contained in the timings of all the quantum jumps.

where $\mathcal{L}(t)$ is a θ -dependent Liouvillian, e.g., $\mathcal{L}(t)\bar{\rho} = -i[H(t), \bar{\rho}]$ in the absence of decoherence or $\mathcal{L}(t)\bar{\rho} = -i[H(t), \bar{\rho}] + \sum_a \gamma_a(t)\mathcal{D}[c_a(t)]\bar{\rho}$ under a general decoherence channel, where $\mathcal{D}[c]\rho \equiv c\rho c^\dagger - \{c^\dagger c, \rho\}/2$ describes the decoherence in the Lindblad form, $\{c_a(t)\}$ are time-dependent quantum jump operators, and $\{\gamma_a(t)\}$ are time-dependent decoherence rates. The final state of the quantum probe is

$$\bar{\rho}(\theta) \equiv \mathcal{T} \exp\left(\int_0^T \mathcal{L}(t)dt\right)\rho_0 \equiv \mathcal{N}_\theta(\rho_0), \quad (2)$$

where \mathcal{T} is the time-ordering superoperator and \mathcal{N}_θ stands for the θ -dependent nonunitary evolution, i.e., the quantum channel, which maps a θ -independent initial state ρ_0 to a θ -dependent final state $\bar{\rho}(\theta)$. The nonunitary nature of the quantum channel is manifested in the fact that the final state is mixed even if the initial state is pure.

Recently, there was remarkable progress in establishing practical bounds on the achievable estimation precision in the presence of decoherence [20,61–69,76,77]. The key idea is to purify the nonunitary quantum channel \mathcal{N}_θ of the quantum probe into a unitary evolution of an extended system consisting of the quantum probe and an environment and then minimize the QFI of the extended system [61,62]. In the following we use this purification formalism to establish a general theory of MQT for an arbitrary environment.

When the environment causing the decoherence is included, the joint evolution of the extended system (consisting of the quantum probe and the environment) during $[0, T]$ is described by a unitary evolution operator $U_{\text{ext}}(\theta)$ and the final state of the extended system is

$$\rho_{\text{ext}}(\theta) \equiv U_{\text{ext}}(\theta)(|E_0\rangle\langle E_0| \otimes \rho_0)U_{\text{ext}}^\dagger(\theta), \quad (3)$$

where $|E_0\rangle$ is the θ -independent initial state of the environment. Therefore, including the environment purifies the nonunitary quantum channel \mathcal{N}_θ of the quantum probe into a unitary evolution of the extended system, which maps a pure initial state $|E_0\rangle \otimes |\psi_0\rangle$ into a pure final state $U_{\text{ext}}(\theta)|E_0\rangle \otimes |\psi_0\rangle$. Tracing out the environmental degree of freedom in an arbitrary orthonormal complete, θ -independent basis $\{|E_l\rangle\}$ gives the reduced density matrix of the quantum probe

$$\bar{\rho}(\theta) = \text{Tr}_E \rho_{\text{ext}}(\theta) = \sum_l \Pi_l(\theta)\rho_0\Pi_l^\dagger(\theta) \equiv \sum_l \tilde{\rho}_l(\theta), \quad (4)$$

where

$$\Pi_l(\theta) \equiv \langle E_l|U_{\text{ext}}(\theta)|E_0\rangle \quad (5)$$

are Kraus operators acting on the quantum probe. Equation (4) gives a representation of the nonunitary quantum channel \mathcal{N}_θ in terms of a set of Kraus operators $\{\Pi_l(\theta)\}$ [61] or equivalently a representation of $\bar{\rho}(\theta) = \mathcal{N}_\theta(\rho_0)$ [see Eq. (2)] in terms of a set of quantum trajectories $\tilde{\rho}_l(\theta) \equiv \Pi_l(\theta)\rho_0\Pi_l^\dagger(\theta)$, which occurs with a probability $P_l(\theta) \equiv \text{Tr} \tilde{\rho}_l(\theta)$. The completeness of the environmental basis $\sum_l |E_l\rangle\langle E_l| = 1$ leads to the completeness of the Kraus operators $\sum_l \Pi_l^\dagger(\theta)\Pi_l(\theta) = 1$ and hence the normalization $\text{Tr} \bar{\rho}(\theta) = \sum_l P_l(\theta) = 1$. For a pure initial state $\rho_0 = |\psi_0\rangle\langle\psi_0|$ of the quantum probe, the final

state of the extended system is

$$|\Psi_{\text{ext}}(\theta)\rangle = U_{\text{ext}}(\theta)|E_0\rangle \otimes |\psi_0\rangle = \sum_l |E_l\rangle \otimes \Pi_l(\theta)|\psi_0\rangle, \quad (6)$$

where $\Pi_l(\theta)|\psi_0\rangle$ is a pure-state quantum trajectory of the quantum probe.

Replacing $U_{\text{ext}}(\theta)$ by $u_E(\theta)U_{\text{ext}}(\theta)$, with $u_E(\theta)$ an arbitrary unitary operator acting on the environment, leaves the quantum channel \mathcal{N}_θ and hence the final state $\bar{\rho}(\theta) = \mathcal{N}_\theta(\rho_0)$ of the quantum probe invariant, but changes $\Pi_l(\theta)$ to

$$\pi_l(\theta) \equiv \langle E_l|u_E(\theta)U_{\text{ext}}(\theta)|E_0\rangle = \sum_{l'} u_{ll'}(\theta)\Pi_{l'}(\theta),$$

where $u_{ll'}(\theta) \equiv \langle E_l|u_E(\theta)|E_{l'}\rangle$ is a unitary matrix, so it gives a different representation of the nonunitary quantum channel \mathcal{N}_θ in terms of a different set of Kraus operators $\{\pi_l(\theta)\}$ or equivalently a representation of $\bar{\rho}(\theta) = \mathcal{N}_\theta(\rho_0)$ in terms of a different set of quantum trajectories $\bar{\rho}(\theta) = \sum_l \pi_l(\theta)\rho_0\pi_l^\dagger(\theta)$. Therefore, the purification (and hence representation) of the nonunitary quantum channel \mathcal{N}_θ is not unique: Given a purification $U_{\text{ext}}(\theta)$ and hence a representation $\{\Pi_l(\theta) \equiv \langle E_l|U_{\text{ext}}(\theta)|E_0\rangle\}$ for \mathcal{N}_θ , exhausting all possible unitaries $u_E(\theta)$ exhausts all possible unitary purifications $u_E(\theta)U_{\text{ext}}(\theta)$ and hence all possible Kraus operator representations $\{\pi_l(\theta) \equiv \sum_{l'} u_{ll'}(\theta)\Pi_{l'}(\theta)\}$ of \mathcal{N}_θ . Physically, this means that there is an infinite number of different environments that lead to the same reduced evolution \mathcal{N}_θ of the quantum probe. Next we consider a hierarchy of constraints on our ability to measure the joint system and derive a hierarchy of inequalities for the precision for estimating θ . In the following we omit the dependences of various quantities on θ for brevity.

B. Hierarchy of estimation precision

Here we consider a fixed environment that purifies the nonunitary evolution \mathcal{N} of the quantum probe into a unitary evolution U_{ext} of the extended system consisting of the quantum probe and the environment. Correspondingly, the final state $\bar{\rho} = \mathcal{N}(\rho_0)$ of the quantum probe is purified into ρ_{ext} in Eq. (3) for the extended system.

First, when arbitrary joint measurements of the extended system are available, we can make an optimal joint measurement (see Appendix A) of the extended system to extract all the QFI $\mathcal{F}[\rho_{\text{ext}}]$ in the final state ρ_{ext} , so the fundamental precision follows from Eq. (1) as

$$\delta\theta_{\text{ext}} \equiv \frac{1}{\sqrt{\nu\mathcal{F}[\rho_{\text{ext}}]}}. \quad (7)$$

This fundamental estimation precision was considered in Refs. [71,72,74] for specific quantum channels, such as a time-homogeneous Markovian quantum channel, as described by a time-homogeneous master equation.

Second, when arbitrary joint measurements are not available, but arbitrary separate measurements of the quantum probe and the environment are available, we can utilize different measurements of the environment to unravel $\bar{\rho}$ into different sets of quantum trajectories [see Fig. 1(b)]. Specifically, a projective measurement of the environment in an arbitrary orthonormal complete, θ -independent basis $\{|E_l\rangle\}$

has a probability $P_l \equiv \text{Tr } \tilde{\rho}_l$ to yield an outcome $|E_l\rangle$ and the occurrence of this outcome collapses the quantum probe into the corresponding quantum trajectory $\tilde{\rho}_l \equiv \Pi_l \rho_0 \Pi_l^\dagger$ [with Π_l given by Eq. (5)], which can be normalized as $\rho_l = \tilde{\rho}_l / P_l$. The average amount of information in the measurement outcome is quantified by the CFI

$$F[\{P_l\}] = \sum_l \frac{(\partial_\theta P_l)^2}{P_l}, \quad (8)$$

while the average amount of information in the quantum trajectory ρ_l is quantified by the QFI $\mathcal{F}[\rho_l]$. The latter can be fully extracted by an optimal measurement of the quantum probe (see Appendix A). Therefore, the average amount of information extracted from a measurement of the environment in the basis $\{|E_l\rangle\}$ and an optimal measurement of the quantum probe is

$$\mathbb{F} \equiv F[\{P_l\}] + \sum_l P_l \mathcal{F}[\rho_l], \quad (9)$$

which coincides with the QFI $\mathcal{F}[\rho_{\text{ext}}\{|E_l\rangle\}]$ in the joint state

$$\rho_{\text{ext}}\{|E_l\rangle\} \equiv \sum_l |E_l\rangle\langle E_l| \otimes \Pi_l \rho_0 \Pi_l^\dagger = \sum_l P_l |E_l\rangle\langle E_l| \otimes \rho_l \quad (10)$$

after measuring the environment in the basis $\{|E_l\rangle\}$. The joint state before the measurement (3) can be written as

$$\rho_{\text{ext}} \equiv \sum_{l'l'} |E_l\rangle\langle E_{l'}| \otimes \Pi_l \rho_0 \Pi_{l'}^\dagger,$$

so the measurement of the environment removes all off-diagonal coherences in the measurement basis $\{|E_l\rangle\}$. After repeating this procedure $\nu \gg 1$ times, we can use the ν outcomes from the measurements of the environment and the ν outcomes from the optimal measurements of the quantum probe to construct an optimal unbiased estimator to θ (see Appendix A). The fundamental estimation precision of this MQT method follows from Eq. (1) as

$$\delta\theta_{\text{MQT}} \equiv \frac{1}{\sqrt{\nu \mathbb{F}}}. \quad (11)$$

In a previous work, Albarelli *et al.* [71] considered homodyne measurement of a Markovian bosonic environment (leading to time-homogeneous Markovian dynamics) and arrived at Eq. (11) for this specific model through straightforward (but somewhat tedious) derivation with the assistance of both the classical Cramér-Rao bound and the quantum Cramér-Rao bound. Here our analysis shows that (i) Eq. (11) is valid for general nonunitary dynamics and general (projective) measurements on the environment and (ii) Eq. (11) follows directly from the quantum Cramér-Rao bound [Eq. (1)]. A similar analysis has been used to discuss quantum parameter estimation with postselection [93].

Third, if only the quantum probe can be measured, then we can use an optimal measurement (see Appendix A) on the quantum probe to extract all the QFI $\mathcal{F}[\bar{\rho}]$ in $\bar{\rho}$, so the estimation precision follows from Eq. (1) as

$$\delta\bar{\theta} \equiv \frac{1}{\sqrt{\nu \mathcal{F}[\bar{\rho}]}}. \quad (12)$$

Since the evolution $\rho_{\text{ext}} \rightarrow \rho_{\text{ext}}\{|E_l\rangle\}$ and $\rho_{\text{ext}}\{|E_l\rangle\} \rightarrow \bar{\rho} = \text{Tr}_E \rho_{\text{ext}}\{|E_l\rangle\}$ are both nonunitary, while no θ -independent quantum operation can increase the QFI [94], we have

$$\mathcal{F}[\rho_{\text{ext}}] \geq \mathbb{F} = \mathcal{F}[\rho_{\text{ext}}\{|E_l\rangle\}] \geq \mathcal{F}[\bar{\rho}] \quad (13)$$

and hence

$$\delta\theta_{\text{ext}} \leq \delta\theta_{\text{MQT}} \leq \delta\bar{\theta}.$$

In the above, $\mathcal{F}[\bar{\rho}]$ ($\mathcal{F}[\rho_{\text{ext}}]$) is uniquely determined by the quantum state $\bar{\rho}$ (ρ_{ext}), while $\rho_{\text{ext}}\{|E_l\rangle\}$ and hence \mathbb{F} still depend on the measurement of the environment. Optimal MQT requires choosing an optimal measurement basis $\{|E_l\rangle\}$ to maximize \mathbb{F} . The second inequality, i.e., $\mathbb{F} \geq \mathcal{F}[\bar{\rho}]$, is just the extended convexity of the QFI [95,96], so our analysis not only provides a physically intuitive proof for the extended convexity of the QFI, but also identifies the physical meaning of \mathbb{F} as the QFI $\mathcal{F}[\rho_{\text{ext}}\{|E_l\rangle\}]$ in the postmeasurement state $\rho_{\text{ext}}\{|E_l\rangle\}$ [93].

Recent work by Albarelli *et al.* [72] gives an equation similar to Eq. (13) for the special case of photon-counting and homodyne measurement of a Markovian bosonic environment. They further conjectured that \mathbb{F} is a nondecreasing function of the measurement efficiency. Here our general formalism allows a simple generalization: Since an imperfect measurement can be regarded as a perfect measurement followed by a nonunitary quantum operation, while any θ -independent quantum operation cannot increase the QFI [94], $\mathcal{F}[\rho_{\text{ext}}\{|E_l\rangle\}]$, and hence \mathbb{F} , is a nondecreasing function of the measurement efficiency of the environment for any environment.

C. Connection to purification-based QFI bounds

Another advantage of our general formalism is that it provides an interesting connection between the MQT approach and the minimization over purification (MOP) technique in quantum parameter estimation [61], which has motivated many works that derive fundamental bounds on the estimation precision [20,62–69,76,77]. In the context of MOP, the aim is to find the maximum of the QFI $\mathcal{F}[\bar{\rho}]$ in the nonselective final state $\bar{\rho} = \mathcal{N}(\rho_0)$ by optimizing the initial state ρ_0 . Due to the convexity of the QFI, the maximum of $\mathcal{F}[\bar{\rho}]$ is always attained by pure initial states, so it suffices to consider $\rho_0 = |\psi_0\rangle\langle\psi_0|$. Even in this case, the final state $\bar{\rho}$ is still mixed, so calculating $\mathcal{F}[\bar{\rho}]$ requires diagonalizing $\bar{\rho}$, which becomes tedious when the Hilbert space of the quantum probe is large. By contrast, for a θ -dependent pure state $|\psi\rangle$, its QFI can be easily evaluated by the formula [89,90] $\mathcal{F}[\psi] = 4(\langle\partial_\theta\psi|\partial_\theta\psi\rangle - \langle\psi|i\partial_\theta\psi\rangle^2)$ (see Appendix A). Interestingly, Escher *et al.* [62] proves a purification-based definition of the QFI:

$$\mathcal{F}[\bar{\rho}] = \min_{\Psi_{\text{ext}}} \mathcal{F}[\Psi_{\text{ext}}] = \min_{\{\Pi_l\}} 4(\langle\psi_0|\alpha|\psi_0\rangle - \langle\psi_0|\beta|\psi_0\rangle^2), \quad (14)$$

where $\alpha \equiv \sum_l (\partial_\theta \Pi_l^\dagger) (\partial_\theta \Pi_l)$ and $\beta \equiv i \sum_l \Pi_l^\dagger \partial_\theta \Pi_l$ are Hermitian operators acting on the quantum probe and the minimization runs over all possible purifications $|\Psi_{\text{ext}}\rangle$ [see Eq. (6)] of $\bar{\rho}$ or equivalently all possible Kraus operator representations of \mathcal{N} . Independently, Fujiwara and Imai [61]

proved

$$\mathcal{F}[\bar{\rho}] = \min_{\Psi_{\text{ext}}} 4 \langle \partial_\theta \Psi_{\text{ext}} | \partial_\theta \Psi_{\text{ext}} \rangle = \min_{\{\Pi_l\}} 4 \langle \psi_0 | \alpha | \psi_0 \rangle. \quad (15)$$

These two definitions are equivalent because the purification that saturates Eq. (15) obeys $\langle \Psi_{\text{ext}} | i \partial_\theta \Psi_{\text{ext}} \rangle = \langle \psi_0 | \beta | \psi_0 \rangle = 0$ [61,67]. An upper bound for the maximal QFI $\max_{\psi_0} \mathcal{F}[\bar{\rho}]$ can be obtained by exchanging \max_{ψ_0} and $\min_{\{\Pi_l\}}$ [63,66–69,77,97],

$$\max_{\psi_0} \mathcal{F}[\bar{\rho}] \leq 4 \min_{\{\Pi_l\}} \|\alpha\|,$$

where $\|A\|$ is the maximal eigenvalue of $\sqrt{A^\dagger A}$. When in addition to the quantum probe access to some ancillas is available, this upper bound is attainable; otherwise this upper bound is not necessarily attainable [61,97].

To make a connection to the MQT method, we notice that when $\rho_0 = |\psi_0\rangle\langle\psi_0|$, the quantum trajectories are pure states $\tilde{\rho}_l = |\tilde{\psi}_l\rangle\langle\tilde{\psi}_l| = P_l |\psi_l\rangle\langle\psi_l|$, where $|\tilde{\psi}_l\rangle \equiv \Pi_l |\psi_0\rangle$ is the unnormalized trajectory, $P_l = \langle \tilde{\psi}_l | \tilde{\psi}_l \rangle$ is the occurrence probability, and $|\psi_l\rangle \equiv |\tilde{\psi}_l\rangle / \sqrt{P_l}$ is the normalized trajectory. The QFI $\mathcal{F}[\Psi_{\text{ext}}]$ in the final state $\rho_{\text{ext}} = |\Psi_{\text{ext}}\rangle\langle\Psi_{\text{ext}}|$ [see Eq. (6)] of the extended system is

$$\begin{aligned} \mathcal{F}[\Psi_{\text{ext}}] &= 4(\langle \psi_0 | \alpha | \psi_0 \rangle - \langle \psi_0 | \beta | \psi_0 \rangle^2) \\ &= F[\{P_l\}] \\ &+ 4 \left[\sum_l P_l \langle \partial_\theta \psi_l | \partial_\theta \psi_l \rangle - \left(\sum_l P_l \langle \psi_l | i \partial_\theta \psi_l \rangle \right)^2 \right]. \end{aligned}$$

For comparison, the QFI in the postmeasurement state $\rho_{\text{ext}|E_l} = \sum_l P_l |E_l\rangle\langle E_l| \otimes |\psi_l\rangle\langle\psi_l|$ of the extended system is

$$\mathbb{F} = \mathcal{F}[\rho_{\text{ext}|E_l}] = F[\{P_l\}] + \sum_l P_l \mathcal{F}[\psi_l],$$

where $\mathcal{F}[\psi_l]$ is the QFI in the normalized trajectory $|\psi_l\rangle$. As discussed in the preceding section, the inequality $\mathcal{F}[\Psi_{\text{ext}}] \geq \mathcal{F}[\rho_{\text{ext}|E_l}]$ [see Eq. (13)] follows from the simple fact that $\rho_{\text{ext}|E_l}$ is obtained from $|\Psi_{\text{ext}}\rangle$ by a nonunitary operation, which cannot increase the QFI [94]. Alternatively, we rewrite their difference as

$$\mathcal{F}[\Psi_{\text{ext}}] - \mathbb{F} = 4(|\mathbf{u}|^2 |\mathbf{v}|^2 - |\mathbf{u} \cdot \mathbf{v}|^2),$$

where \mathbf{u} and \mathbf{v} are two real vectors $(\mathbf{u})_l = \sqrt{P_l}$ and $(\mathbf{v})_l = \sqrt{P_l} \langle \psi_l | i \partial_\theta \psi_l \rangle$. Therefore, the inequality $\mathcal{F}[\Psi_{\text{ext}}] \geq \mathbb{F}$ simply follows from the Cauchy-Schwarz inequality. This inequality is saturated if and only if $\mathbf{u} \propto \mathbf{v}$, i.e., when

$$\langle \psi_l | \partial_\theta \psi_l \rangle = \lambda(\theta), \quad (16)$$

where $\lambda(\theta)$ is an arbitrary l -independent constant.

Now we discuss the connection and distinction between the MOP technique and the MQT method. In the context of MOP, the ultimate goal is to derive the tightest upper bound for the maximal QFI $\max_{\psi_0} \mathcal{F}[\bar{\rho}]$, which characterizes the fundamental precision for estimating the parameter θ of a given quantum channel \mathcal{N} without any access to the environment. As a result, the environment, the purification $|\Psi_{\text{ext}}\rangle$, and the QFI $\mathcal{F}[\Psi_{\text{ext}}]$ are not physical objects but instead mathematical tools for converting the direct evaluation of the mixed-state QFI $\mathcal{F}[\bar{\rho}]$ to a minimization problem: $\mathcal{F}[\bar{\rho}] =$

$\min_{\Psi_{\text{ext}}} \mathcal{F}[\Psi_{\text{ext}}]$. The key physics is that the quantum channel \mathcal{N} and hence the final state $\bar{\rho} = \mathcal{N}(|\psi_0\rangle\langle\psi_0|)$ can be generated by an infinite number of fictitious environments. Each distinct environment corresponds to a distinct joint unitary evolution U_{ext} and hence a distinct Kraus operator representation $\{\Pi_l\}$ [see Eq. (5)] of \mathcal{N} and a distinct purification $|\Psi_{\text{ext}}\rangle$ [see Eq. (6)] of $\bar{\rho}$. The purification-based definitions of the QFI [Eq. (14) or (15)] dictate that (i) $\mathcal{F}[\Psi_{\text{ext}}] \geq \mathcal{F}[\bar{\rho}]$, i.e., including the environment never decreases the QFI, and (ii) there exist QFI-preserving environments for which the joint state $|\Psi_{\text{ext}}\rangle$ contains the same QFI as the reduced state $\mathcal{F}[\Psi_{\text{ext}}] = \mathcal{F}[\bar{\rho}]$.

By contrast, in the context of the MQT method, we assume that we have access to the physical environment that is coupled to the quantum probe. In this case, the quantum probe and the physical environment undergo physical unitary evolution U_{ext} as determined by their physical Hamiltonians and mutual couplings, so we no longer have any degree of freedom to choose the environment. Here the joint state $|\Psi_{\text{ext}}\rangle$ and its QFI $\mathcal{F}[\Psi_{\text{ext}}]$ are completely determined by the initial state $|\psi_0\rangle$ of the quantum probe, while $\mathbb{F} = \mathcal{F}[\rho_{\text{ext}|E_l}]$ also depends on the basis $\{|E_l\rangle\}$ of the measurement of the environment. The ultimate goal is to optimize the initial state $|\psi_0\rangle$ and the measurement basis $\{|E_l\rangle\}$ for maximal \mathbb{F} , e.g., if we can find a suitable basis that satisfies Eq. (16), then \mathbb{F} attains its maximum $\mathcal{F}[\Psi_{\text{ext}}]$. Interestingly, the purification-based definition of the QFI suggests that when the physical environment happens to be QFI preserving, i.e., $\mathcal{F}[\Psi_{\text{ext}}] = \mathcal{F}[\bar{\rho}]$, then Eq. (13) dictates $\mathcal{F}[\Psi_{\text{ext}}] = \mathbb{F} = \mathcal{F}[\bar{\rho}]$ and hence $\delta\theta_{\text{ext}} = \delta\theta_{\text{MQT}} = \delta\bar{\theta}$, i.e., including the environment provides no advantage in improving the estimation precision.

D. Superoperator approach for Markovian dynamics

Here we consider homogeneous Markovian quantum channel $\mathcal{N} = e^{\mathcal{L}T}$ described by a time-independent Liouvillian \mathcal{L} , e.g., $\mathcal{L}\bar{\rho} = -i[H, \bar{\rho}]$ in the absence of decoherence or $\mathcal{L}\bar{\rho} = -i[H, \bar{\rho}] + \sum_a \gamma_a \mathcal{D}[c_a]\bar{\rho}$ in the presence of decoherence. With all detectable quantum jumps [98–105] denoted by the superoperator \mathcal{J} (see the next section for an example), \mathcal{L} becomes the sum of \mathcal{J} and $\mathcal{L}_0 \equiv \mathcal{L} - \mathcal{J}$ and the nonselective final state of the quantum probe unravels into all possible quantum trajectories [cf. Eq. (4)]

$$\bar{\rho} = \tilde{\rho}_\emptyset + \int_0^T dt_1 \tilde{\rho}_{t_1} + \int_0^T dt_2 \int_0^{t_2} dt_1 \tilde{\rho}_{t_1 t_2} + \dots, \quad (17)$$

where

$$\tilde{\rho}_\emptyset \equiv e^{\mathcal{L}_0 T} \rho_0$$

is the trajectory with no quantum jump,

$$\tilde{\rho}_{t_1} \equiv e^{\mathcal{L}_0(T-t_1)} \mathcal{J} e^{\mathcal{L}_0 t_1} \rho_0$$

is the trajectory with one exclusive quantum jump at t_1 ,

$$\tilde{\rho}_{t_1 t_2} \equiv e^{\mathcal{L}_0(T-t_2)} \mathcal{J} e^{\mathcal{L}_0(t_2-t_1)} \mathcal{J} e^{\mathcal{L}_0 t_1} \rho_0$$

is the trajectory with two exclusive quantum jumps at t_1 and t_2 , etc. The trace of each quantum trajectory gives its occurrence probability (density), e.g., the jumpless trajectory occurs with a probability $P_\emptyset \equiv \text{Tr} \tilde{\rho}_\emptyset$, the trajectory $\tilde{\rho}_{t_1}$ occurs with a probability density $p_{t_1} \equiv \text{Tr} \tilde{\rho}_{t_1}$, the trajectory $\tilde{\rho}_{t_1 t_2}$ occurs with

a probability density $p_{t_1 t_2} \equiv \text{Tr} \tilde{\rho}_{t_1 t_2}$, etc. The normalization $\text{Tr} \tilde{\rho} = 1$ leads to the normalization of all the probabilities

$$P_{\mathcal{O}} + \int_0^T p_{t_1} dt_1 + \int_0^T dt_2 \int_0^{t_2} dt_1 p_{t_1 t_2} + \dots = 1.$$

These analytical expressions for the quantum trajectories in terms of the quantum jump superoperator \mathcal{J} and jumpless evolution superoperator \mathcal{L}_0 correspond to an exact integration of the stochastic master equation [71,72].

In MQT, we not only track the quantum trajectory, but also record the timing of every observed quantum jump during the evolution [see Fig. 1(b)]. At the end of the evolution, we make an optimal measurement of the quantum probe to transfer all the QFI in the quantum probe into the measurement outcome. After repeating this measurement cycle $\nu \gg 1$ times, we can use all the observed timings and the ν measurement outcomes to construct an optimal unbiased estimator to θ (see Appendix A). The fundamental precision is given by Eq. (11), where $\mathbb{F} = F + \bar{\mathcal{F}}$ [cf. Eq. (9)] is the sum of the CFI [cf. Eq. (8)]

$$F = \frac{(\partial_{\theta} P_{\mathcal{O}})^2}{P_{\mathcal{O}}} + \int_0^T \frac{(\partial_{\theta} p_{t_1})^2}{p_{t_1}} dt_1 + \dots \quad (18)$$

contained in all the timings of the quantum jumps and the trajectory-averaged QFI

$$\bar{\mathcal{F}} \equiv P_{\mathcal{O}} \mathcal{F}[\rho_{\mathcal{O}}] + \int_0^T p_{t_1} \mathcal{F}[\rho_{t_1}] dt_1 + \dots, \quad (19)$$

where $\rho_{\mathcal{O}} \equiv \tilde{\rho}_{\mathcal{O}}/P_{\mathcal{O}}$, $\rho_{t_1} \equiv \tilde{\rho}_{t_1}/p_{t_1}$, etc., are normalized quantum trajectories.

For the estimation of Hamiltonian parameters, the jumpless trajectory $\tilde{\rho}_{\mathcal{O}}$ is less (usually not) influenced by the decoherence, so its QFI is much higher than other trajectories and the nonselective state $\tilde{\rho}$. When $[\mathcal{J}, \mathcal{L}_0] = 0$, we have $\tilde{\rho}_{t_1 \dots t_n} \equiv \mathcal{J}^n \tilde{\rho}_{\mathcal{O}}$ and $\tilde{\rho} = e^{\mathcal{J}T} \tilde{\rho}_{\mathcal{O}}$, i.e., all the quantum jumps can be deferred after the jumpless evolution. If \mathcal{J} further preserves the QFI, then all the quantum trajectories contain the same QFI as the jumpless trajectory, so $\mathbb{F} \geq \mathcal{F}[\rho_{\mathcal{O}}]$ and $\delta\theta_{\text{MQT}} \leq 1/\sqrt{\nu \mathcal{F}[\rho_{\mathcal{O}}]}$.

The capability of MQT to resolve different quantum trajectories motivates a probabilistic protocol by postselection of quantum trajectories. In this protocol, after resolving the quantum trajectories, we only perform optimal measurements of high-QFI trajectories and then construct an optimal unbiased estimator based on the outcomes of these measurements, while discarding all zero-QFI and even low-QFI trajectories. On one hand, this treatment reduces the workload of performing a large number of optimal measurements and constructing optimal unbiased estimators from a large number of measurement outcomes (see Appendix A). On the other hand, discarding any trajectory with nonzero QFI will degrade the fundamental estimation precision. Therefore, one can balance between the estimation precision and the cost of measurement and data postprocessing to optimize the whole parameter estimation process. A similar situation has been encountered in other probabilistic metrology protocols such as weak-value amplification [106,107], where postselection gains technical advantages in data processing [108] at the cost of degrading the fundamental estimation precision [93,109].

E. Monitoring quantum trajectories via noiseless ancillas: Connection to QEC

In most cases, MQT requires direct measurement of the noisy environment, an experimentally challenging task for realistic noise processes. Fortunately, when the Hamiltonian evolution and the decoherence channel satisfy certain conditions, it is possible to achieve MQT by quantum error encoding and error detection assisted by noiseless ancillas [21–23,69], i.e., we can use QEC to resolve the quantum trajectories, but do not apply any corrective operations. Such QEC-based MQT can be regarded as a QEC protocol without corrective operations, so it is less powerful than the full QEC-based metrology [21–28,68,69]. Nevertheless, MQT itself provides an interesting insight into how the information leaks into the distinct quantum trajectories and how they are recovered. Moreover, for very special cases where corrective operations are not necessary (see Appendix B for an example), MQT becomes advantageous as it avoids faulty corrective operations [22].

We begin with a simple example: monitoring the spin-flip channel of a spin 1/2 in the Lindblad form $d\tilde{\rho}(t)/dt = \gamma \mathcal{D}[S_x] \tilde{\rho}(t)$. Here the quantum jump operator S_x induce random jumps between $|\uparrow\rangle$ and $|\downarrow\rangle$. These random jumps can be monitored via the QEC protocol [22], which adds an ancilla that is not affected by the noise. Physically, this can be realized in a nitrogen-vacancy center [8,110], where the electron spin serves as the quantum probe spin 1/2 and the ^{15}N nuclear spin serves as the ancilla. We use $|\uparrow\rangle$ and $|\downarrow\rangle$ for the spin 1/2, $|0\rangle$ and $|1\rangle$ for the ancilla, σ_z for the Pauli matrix on the spin 1/2, and $\sigma_z^{(a)}$ for the Pauli matrix on the ancilla: $\sigma_z^{(a)}|0\rangle = |0\rangle$ and $\sigma_z^{(a)}|1\rangle = -|1\rangle$. The syndrome operator is $\Sigma \equiv \sigma_z \sigma_z^{(a)}$. The code subspace spanned by $|\uparrow\rangle|0\rangle$ and $|\downarrow\rangle|1\rangle$ is the eigensubspace of the syndrome operator with eigenvalue +1, so we denote the code subspace by Σ_+ . The occurrence of a spin flip maps the code subspace Σ_+ onto an orthogonal error subspace as spanned by $|\downarrow\rangle|0\rangle$ and $|\uparrow\rangle|1\rangle$. This error subspace is an eigensubspace of the syndrome operator Σ with eigenvalue -1 , so we denote it by Σ_- . The occurrence of another spin flip maps Σ_- back to Σ_+ . Therefore, frequently measuring the syndrome operator Σ allows us to monitor the spin flip in real time. For Hamiltonian parameter estimation, if the Hamiltonian commutes with Σ and hence leaves Σ_{\pm} invariant, then monitoring the spin flip does not affect the coherent Hamiltonian evolution. As an example, we consider $H = \omega S_z$, with ω the unknown parameter to be estimated. The total nonselective evolution is $d\tilde{\rho}(t)/dt = -i[H, \tilde{\rho}(t)] + \gamma \mathcal{D}[S_x] \tilde{\rho}(t)$. Starting from an initial state $|\psi_0\rangle = a|\uparrow\rangle|0\rangle + b|\downarrow\rangle|1\rangle \in \Sigma_+$, in the absence of quantum jumps, the Hamiltonian evolution keeps the state inside Σ_+ : $|\psi(t)\rangle = a|\uparrow\rangle|0\rangle + e^{i\omega t} b|\downarrow\rangle|1\rangle$. The occurrence of a quantum jump at t_0 maps $|\psi(t_0)\rangle$ to $|\tilde{\psi}(t_0)\rangle = a|\downarrow\rangle|0\rangle + e^{i\omega t_0} b|\uparrow\rangle|1\rangle \in \Sigma_-$, which can be detected as a sign switch of Σ . The subsequent Hamiltonian evolution keeps the state inside Σ_- : $|\tilde{\psi}(t)\rangle = a|\downarrow\rangle|0\rangle + e^{i\omega(t-t_0)} b|\uparrow\rangle|1\rangle$. The occurrence of another quantum jump at t_1 maps $|\tilde{\psi}(t_1)\rangle$ back to the code subspace $|\psi(t_1)\rangle = a|\uparrow\rangle|0\rangle + e^{i\omega(t_0-t_1)} b|\downarrow\rangle|1\rangle \in \Sigma_+$, which can be detected as another sign switch of Σ . Here, in contrast to the full QEC protocols [21–27], we only monitor the quantum trajectory without applying any corrective operations.

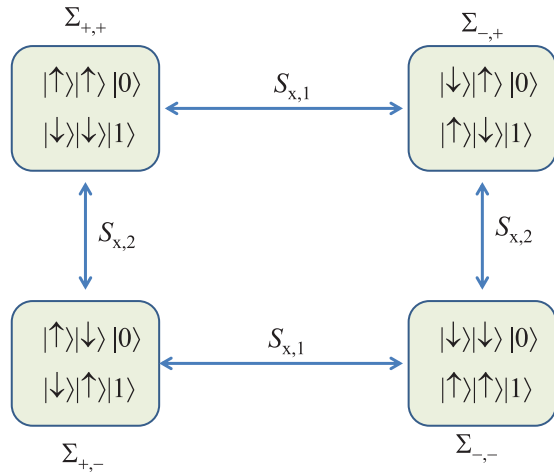


FIG. 2. QEC-based MQT for two spins 1/2 with the assistance of a noiseless ancilla. The four distinct eigensubspaces of the two-component syndrome operator $\Sigma = (\sigma_z^{(1)}\sigma_z^{(a)}, \sigma_z^{(2)}\sigma_z^{(a)})$ define the code subspace $\Sigma_{+,+}$ and three error subspaces $\Sigma_{-,+}$, $\Sigma_{+,-}$, and $\Sigma_{-,-}$. Different subspaces are connected by the flip of individual spins.

The following are the key ingredients of this QEC-based MQT. (i) The code subspace Σ_+ and the error subspace Σ_- are eigensubspaces of the syndrome operator Σ with distinct eigenvalues. (ii) The quantum jump operator anticommutes with the syndrome operator, so it maps an eigenstate of the syndrome operator to another eigenstate with an opposite eigenvalue, i.e., it induces the transition between Σ_+ and Σ_- and hence can be detected by measuring the syndrome operator [111]. If, in addition, the Hamiltonian commutes with the syndrome operator so that the Hamiltonian evolution leaves Σ_+ and Σ_- invariant, then the detection of the quantum jump does not affect the Hamiltonian evolution, similar to the full QEC-based metrology [22,26]. For example, a single noiseless ancilla allows us to monitor the spin flip of an arbitrary number N of spins 1/2 by using the N -component syndrome operator $\Sigma \equiv (\sigma_z^{(1)}\sigma_z^{(a)}, \dots, \sigma_z^{(N)}\sigma_z^{(a)})$, where $\sigma_z^{(i)}$ is the Pauli operator for the i th spin 1/2 and the flip of the i th spin 1/2 is detected as the sign switch of the i th component $\sigma_z^{(i)}\sigma_z^{(a)}$ (see Fig. 2 for an example for $N = 2$). When the Hamiltonian leaves each eigensubspace invariant, e.g., $H = \omega(S_z^{(1)} + \dots + S_z^{(N)})$, MQT does not affect the Hamiltonian evolution.

The requirement that MQT leave the Hamiltonian evolution intact can be satisfied only when the Hamiltonian is completely transversal to the quantum jump operator [2] (e.g., ωS_z is transversal to S_x in our example). Generally, the Hamiltonian is the sum of a transversal component H_\perp (i.e., the component outside the Lindblad span of the decoherence channel [68,69]) and a parallel component H_\parallel (i.e., the component inside the Lindblad span of the decoherence channel [68,69]): The former keeps each eigensubspace of the syndrome operator invariant, while the latter (as well as the quantum jump) can induce transitions between different eigensubspaces. However, frequent measurement of the syndrome operator leads to the quantum Zeno effect that effectively suppresses H_\parallel so that only H_\perp survives [69]. In this case, MQT changes the intrinsic Hamiltonian evolution

and hence cannot reveal the intrinsic evolution of the quantum trajectories.

The discussion above suggests that for Hamiltonian parameter estimation, there is an interesting connection between QEC-based MQT and the full QEC-based metrology [68,69]. (i) When $H_\perp = 0$, the QEC-based MQT will completely freeze the Hamiltonian evolution, so the full QEC protocol is not applicable to improve the estimation precision. (ii) When $H_\perp \neq 0$, the QEC-based MQT will suppress H_\parallel but leave H_\perp intact, so the full QEC protocol can recover the Heisenberg scaling of the estimation precision in the noiseless case [68,69]. In particular, when $H_\parallel = 0$, the QEC-based MQT leaves the Hamiltonian evolution intact, so the full QEC protocol can fully recover the estimation precision in the noiseless case [68,69].

III. APPLICATION TO SPIN 1/2

We consider a spin 1/2 \mathbf{S} undergoing the nonselective evolution $\dot{\rho}(t) = \mathcal{L}\rho(t)$ starting from a general initial state

$$\rho_0 = \begin{bmatrix} \rho_{\uparrow\uparrow} & \rho_{\uparrow\downarrow} \\ \rho_{\uparrow\downarrow}^* & \rho_{\downarrow\downarrow} \end{bmatrix},$$

with $\rho_{\downarrow\downarrow} \equiv 1 - \rho_{\uparrow\uparrow}$, where $\mathcal{L}\rho \equiv -i[\omega S_z, \rho] + \gamma \mathcal{D}[c]\rho$, S_z is the z component of the spin, ω is the level splitting, c represents an arbitrary quantum jump operator, and γ is the decoherence rate. Monitoring the quantum jump $\mathcal{J}\rho \equiv \gamma c \rho c^\dagger$ amounts to decomposing \mathcal{L} into the quantum jump \mathcal{J} and the jumpless evolution $e^{\mathcal{L}t}\rho = e^{-i\tilde{H}t}\rho e^{i\tilde{H}^\dagger t}$, where

$$\tilde{H} \equiv \omega S_z - i\frac{\gamma}{2}c^\dagger c$$

is an effective non-Hermitian Hamiltonian that governs the jumpless trajectory $\tilde{\rho}_\circ = e^{\mathcal{L}t}\rho_0$. We consider the estimation of the level splitting ω or the decoherence rate γ (at $\omega = 0$) under three decoherence channels: spin relaxation $c = S_- = |\downarrow\rangle\langle\uparrow|$, spin flip $c = S_x$, and spin dephasing $c = S_z$. We use a subscript $\omega(\gamma)$ to denote the information about $\omega(\gamma)$, e.g., the CFI about $\omega(\gamma)$ is $F_\omega(F_\gamma)$ and the total information about $\omega(\gamma)$ from MQT is $\mathbb{F}_\omega(\mathbb{F}_\gamma)$.

For the spin-relaxation channel, QEC-based MQT is not possible, so MQT requires direct measurement of the environment, which is experimentally challenging for many realistic environments. For the special environment, i.e., the single-mode cavity, the spin relaxation due to the cavity field is always accompanied by the emission of a cavity photon, so it can be monitored by using a photon detector to measure the cavity output [29]. For the spin-flip channel, the Hamiltonian $H = \omega S_z$ is completely transversal to the quantum jump S_x , so QEC-based MQT is applicable and the syndrome operator is $\Sigma \equiv \sigma_z \sigma_z^{(a)}$ (see Sec. II E). For the spin-dephasing channel, the Hamiltonian $H = \omega S_z$ completely lies in the Lindblad span [68,69] of the decoherence channel, i.e., $H_\perp = 0$, so QEC-based MQT will completely freeze the Hamiltonian evolution. Therefore, only when $\omega = 0$ can the QEC-based MQT be used to estimate γ and, in this case, the results for \mathbb{F}_γ are identical to the spin-flip channel since S_z and S_x are connected by a unitary $\pi/2$ rotation around the y axis. In other cases, MQT requires directly monitoring the environment, which may be experimentally challenging. In Appendix B

we give an example for using QEC-based MQT to recover the Heisenberg scaling of frequency estimation for *multiple* qubits.

In a recent work, Albarelli *et al.* [71] considered the fundamental estimation precision of frequency by directly monitoring the radiation field from an ensemble of atoms undergoing Markovian collective dephasing. Another work by Albarelli *et al.* [72] further includes the Markovian spin-flip channel and demonstrated the interesting possibility of recovering the Heisenberg scaling of the estimation precision with respect to the number N of atoms. These works focus on frequency estimation and its scaling with respect to the number N of atoms and rely on either the Gaussian approximation in the limit of a large number of atoms [71] or numerical integration of the stochastic master equation [72]. Here we focus on the time scaling of the estimation precision for both the frequency ω and the dissipation rate γ of a single spin 1/2. Moreover, the superoperator formalism in Sec. IID allows us to obtain explicit analytical expressions. In the following we first give the quantum trajectories and their information content for each decoherence channel and then discuss the estimation precision for ω and γ .

A. Quantum trajectories and Fisher information

For the spin-relaxation channel, $\tilde{H} = \omega S_z - i(\gamma/2)|\uparrow\rangle\langle\uparrow| + i(\gamma/2)|\downarrow\rangle\langle\downarrow|$ and $\mathcal{J}^2 = 0$, so the spin can undergo at most one quantum

jump. The jumpless trajectory is

$$\tilde{\rho}_\emptyset = \begin{bmatrix} e^{-\gamma T} \rho_{\uparrow\uparrow} & e^{-\gamma T/2} e^{-i\omega T} \rho_{\uparrow\downarrow} \\ e^{-\gamma T/2} e^{i\omega T} \rho_{\uparrow\downarrow}^* & \rho_{\downarrow\downarrow} \end{bmatrix}. \quad (20)$$

The trajectory with an exclusive quantum jump at t_1 is $\tilde{\rho}_{t_1} = \gamma e^{-\gamma t_1} \rho_{\uparrow\uparrow} |\downarrow\rangle\langle\downarrow|$. Other trajectories $\tilde{\rho}_{t_1 \dots t_n}$ with $n \geq 2$ quantum jumps are absent. The sum of all the quantum trajectories gives the nonselective density matrix

$$\tilde{\rho} = \begin{bmatrix} e^{-\gamma T} \rho_{\uparrow\uparrow} & e^{-\gamma T/2} e^{-i\omega T} \rho_{\uparrow\downarrow} \\ e^{-\gamma T/2} e^{i\omega T} \rho_{\uparrow\downarrow}^* & 1 - \rho_{\uparrow\uparrow} e^{-\gamma T} \end{bmatrix}. \quad (21)$$

For the spin-flip channel, $\tilde{H} = \omega S_z - i(\gamma/8)$ and $\mathcal{J}^2 = (\gamma/4)^2$, so an arbitrary number of quantum jumps is possible. The jumpless trajectory is

$$\tilde{\rho}_\emptyset = e^{-\gamma T/4} \begin{bmatrix} \rho_{\uparrow\uparrow} & e^{-i\omega T} \rho_{\uparrow\downarrow} \\ e^{i\omega T} \rho_{\uparrow\downarrow}^* & \rho_{\downarrow\downarrow} \end{bmatrix}. \quad (22)$$

The trajectory with n quantum jumps at t_1, \dots, t_n is

$$\tilde{\rho}_{t_1 \dots t_n} = \left(\frac{\gamma}{4}\right)^n e^{-\gamma T/4} \begin{bmatrix} \rho_{\uparrow\uparrow} & \rho_{\uparrow\downarrow} \exp\left(-i\omega \int_0^T s(t) dt\right) \\ \rho_{\uparrow\downarrow}^* \exp\left(i\omega \int_0^T s(t) dt\right) & \rho_{\downarrow\downarrow} \end{bmatrix} \quad (23)$$

for even n and $\sigma_x \tilde{\rho}_{t_1 \dots t_n} \sigma_x$ for odd n , where σ_x is the Pauli matrix and $s(t)$ starts from +1 at $t = 0$ and reverses its sign at t_1, \dots, t_n . The sum of all the trajectories gives the nonselective final state

$$\tilde{\rho} = \begin{bmatrix} \frac{1}{2} + \frac{e^{-\gamma T/2}}{2} (\rho_{\uparrow\uparrow} - \rho_{\downarrow\downarrow}) & (f \rho_{\uparrow\downarrow} + g \rho_{\uparrow\downarrow}^*) e^{-\gamma T/4} \\ (f^* \rho_{\uparrow\downarrow}^* + g \rho_{\uparrow\downarrow}) e^{-\gamma T/4} & \frac{1}{2} - \frac{e^{-\gamma T/2}}{2} (\rho_{\uparrow\uparrow} - \rho_{\downarrow\downarrow}) \end{bmatrix}, \quad (24)$$

where $f = \cos(wT) - i(\omega/w) \sin(wT)$ and $g = \gamma \sin(wT)/4w$ with $w \equiv \sqrt{\omega^2 - (\gamma/4)^2}$.

For the spin-dephasing channel, $\tilde{H} = \omega S_z - i(\gamma/8)$ and $\mathcal{J}^2 = (\gamma/4)^2$, so an arbitrary number of quantum jumps is possible. The jumpless trajectory is the same as the spin-flip channel. The trajectory with n quantum jumps at t_1, \dots, t_n is

$$\tilde{\rho}_{t_1 \dots t_n} = \left(\frac{\gamma}{4}\right)^n e^{-\gamma T/4} \begin{bmatrix} \rho_{\uparrow\uparrow} & (-1)^n \rho_{\uparrow\downarrow} e^{-i\omega T} \\ (-1)^n \rho_{\uparrow\downarrow}^* e^{i\omega T} & \rho_{\downarrow\downarrow} \end{bmatrix}, \quad (25)$$

which is independent of the timings of the n quantum jumps. Summing all the trajectories gives the nonselective final state

$$\tilde{\rho} = \begin{bmatrix} \rho_{\uparrow\uparrow} & e^{-\gamma T/2} e^{-i\omega T} \rho_{\uparrow\downarrow} \\ e^{-\gamma T/2} e^{i\omega T} \rho_{\uparrow\downarrow}^* & \rho_{\downarrow\downarrow} \end{bmatrix}. \quad (26)$$

In Table I we list the information for estimating ω and for estimating γ at $\omega = 0$ for each decoherence channel. In the MQT approach, after ν repeated measurement cycles, the estimation precision

$$\delta\theta = \frac{1}{\sqrt{\nu \mathbb{F}_\theta}} \quad (27)$$

is determined by the total information \mathbb{F}_θ ($\theta = \omega$ or γ) from each measurement cycle. In the conventional approach, after ν repeated measurement cycles, the estimation precision

$$\delta\bar{\theta} = \frac{1}{\sqrt{\nu \mathcal{F}_\theta[\bar{\rho}]}} \quad (28)$$

is determined by the QFI $\mathcal{F}_\theta[\bar{\rho}]$ ($\theta = \omega$ or γ) of the nonselective final state $\bar{\rho}$ in each measurement cycle. According to Eq. (13), we always have $\mathbb{F}_\theta \geq \mathcal{F}_\theta[\bar{\rho}]$, so MQT always improve the estimation precision, but the degree of improvement depends on the parameter to be estimated and the decoherence channel.

From Table I we see that estimating the Hamiltonian parameter ω is very different from estimating the decoherence parameter γ (at $\omega = 0$).

(i) For all the decoherence channels, the CFI about ω (γ) is zero (nonzero), i.e., the timings of the quantum jumps contain information about γ , but no information about ω . Physically, γ characterizes the rate of the quantum jump, so

TABLE I. Information about the qubit frequency ω or the decoherence rate γ (at $\omega = 0$) under different decoherence channels, where $s(t)$ starts from $+1$ at $t = 0$ and switches its sign at every quantum jump (t_1, \dots, t_n) and ρ_{++}, ρ_{--} , and ρ_{+-} are matrix elements of the initial state ρ_0 in the basis $|\pm\rangle \equiv (|\uparrow\rangle \pm |\downarrow\rangle)/\sqrt{2}$. The expression for $\mathcal{F}_\omega[\bar{\rho}]$ under the spin-flip channel is valid up to leading order of γ/ω .

Information about ω	Spin-relaxation channel ($c = S_-$)	Spin-flip channel ($c = S_x$)	Spin-dephasing channel ($c = S_z$)
$\mathcal{F}_\omega[\rho_\otimes]$	$\frac{4T^2 \rho_{\uparrow\downarrow} ^2e^{-\gamma T}}{(\rho_{\uparrow\uparrow}e^{-\gamma T} + \rho_{\downarrow\downarrow})^2}$	$4T^2 \rho_{\uparrow\downarrow} ^2$	$4T^2 \rho_{\uparrow\downarrow} ^2$
$\mathcal{F}_\omega[\rho_{t_1 \dots t_n}]$	0	$4\left[\int_0^T s(t)dt\right]^2 \rho_{\uparrow\downarrow} ^2$	$4T^2 \rho_{\uparrow\downarrow} ^2$
F_ω	0	0	0
$\mathbb{F}_\omega = \bar{\mathcal{F}}_\omega$	$\frac{4T^2 \rho_{\uparrow\downarrow} ^2e^{-\gamma T}}{\rho_{\uparrow\uparrow}e^{-\gamma T} + \rho_{\downarrow\downarrow}}$	$\frac{32 \rho_{\uparrow\downarrow} ^2}{\gamma^2}\left(\frac{\gamma T}{2} - (1 - e^{-\gamma T/2})\right)$	$4T^2 \rho_{\uparrow\downarrow} ^2$
$\mathcal{F}_\omega[\bar{\rho}]$	$4T^2 \rho_{\uparrow\downarrow} ^2e^{-\gamma T}$	$4T^2 \rho_{\uparrow\downarrow} ^2e^{-\gamma T/2}$	$4T^2 \rho_{\uparrow\downarrow} ^2e^{-\gamma T}$
Information about γ at $\omega = 0$	Spin-relaxation channel ($c = S_-$)	Spin-flip channel ($c = S_x$)	Spin-dephasing channel ($c = S_z$)
$\mathcal{F}_\gamma[\rho_\otimes]$	$\frac{T^2\rho_{\uparrow\uparrow}\rho_{\downarrow\downarrow}e^{-\gamma T}}{(\rho_{\uparrow\uparrow}e^{-\gamma T} + \rho_{\downarrow\downarrow})^2}$	0	0
$\mathcal{F}_\gamma[\rho_{t_1 \dots t_n}]$	0	0	0
F_γ	$\frac{\rho_{\uparrow\uparrow}(1 - e^{-\gamma T})}{\gamma^2} - \frac{T^2\rho_{\uparrow\uparrow}\rho_{\downarrow\downarrow}e^{-\gamma T}}{\rho_{\uparrow\uparrow}e^{-\gamma T} + \rho_{\downarrow\downarrow}}$	$\frac{T}{4\gamma}$	$\frac{T}{4\gamma}$
\mathbb{F}_γ	$\frac{\rho_{\uparrow\uparrow}}{\gamma^2}(1 - e^{-\gamma T})$	$\frac{T}{4\gamma}$	$\frac{T}{4\gamma}$
$\mathcal{F}_\gamma[\bar{\rho}]$	$\frac{T^2\rho_{\uparrow\uparrow} \rho_{\uparrow\uparrow} - \rho_{\downarrow\downarrow} ^2(\rho_{\uparrow\uparrow}e^{-\gamma T} + 1)e^{-\gamma T}}{\rho_{\uparrow\uparrow}(1 - \rho_{\uparrow\uparrow}e^{-\gamma T}) - \rho_{\uparrow\downarrow} ^2}$	$\frac{T^2 \rho_{+-} ^2e^{-\gamma T}\rho_{++}\rho_{--}}{\rho_{++}\rho_{--} - \rho_{+-} ^2e^{-\gamma T}}$	$\frac{T^2 \rho_{\uparrow\downarrow} ^2e^{-\gamma T}\rho_{\uparrow\uparrow}\rho_{\downarrow\downarrow}}{\rho_{\uparrow\uparrow}\rho_{\downarrow\downarrow} - \rho_{\uparrow\downarrow} ^2e^{-\gamma T}}$

the occurrence probabilities of all the quantum trajectories depend on γ , but are independent of ω , leading to nonzero F_γ but vanishing F_ω according to Eq. (18). Therefore, for estimating ω , we do not need to record the timings of the quantum jumps.

(ii) For the spin-flip and spin-dephasing channels, the QFI about ω (γ) is nonzero (zero) for all the trajectories. Physically, the dependence of the *normalized* quantum trajectories on ω and γ originates from the jumpless evolution \mathcal{L}_0 or equivalently $\hat{H} = \omega S_z - i(\gamma/8)$, which imprints the ω dependence but no γ dependence onto the normalized quantum trajectories. Therefore, for estimating γ , we only need to record the timings of the quantum jumps, while measurements over the final state are not necessary.

(iii) For the spin-relaxation channel, the trajectory with quantum jumps has vanishing QFI about ω and γ , because a single quantum jump projects an arbitrary state into $|\downarrow\rangle$ and hence eliminates all the information. Therefore, once a quantum jump is detected, we can immediately stop the current measurement cycle and start the next measurement cycle to reduce the total time cost.

(iv) The information about ω is all proportional to $|\rho_{\uparrow\downarrow}|^2$, i.e., the projection of the initial spin in the xy plane, because ω is imprinted onto the quantum probe through the Larmor precession around the z axis. The positive definiteness of the density matrix dictates $|\rho_{\uparrow\downarrow}|^2 \leq \rho_{\uparrow\uparrow}\rho_{\downarrow\downarrow}$, so in the following we set $|\rho_{\uparrow\downarrow}|^2 = \rho_{\uparrow\uparrow}\rho_{\downarrow\downarrow}$ to optimize the estimation precision for ω .

B. Estimation of ω

For the spin-relaxation channel, the jumpless trajectory [Eq. (20)] contains the QFI

$$\mathcal{F}_\omega[\rho_\otimes] = 4T^2 \frac{\rho_{\uparrow\uparrow}e^{-\gamma T}\rho_{\downarrow\downarrow}}{(\rho_{\uparrow\uparrow}e^{-\gamma T} + \rho_{\downarrow\downarrow})^2}$$

and occurs with a probability $P_\otimes(T) = \rho_{\uparrow\uparrow}e^{-\gamma T} + \rho_{\downarrow\downarrow}$, while the trajectories with a quantum jump contains no QFI. Given an arbitrary evolution time T , preparing the initial state $\rho_{\downarrow\downarrow} = 1 - \rho_{\uparrow\uparrow} = 1/(e^{\gamma T} + 1)$ makes the QFI of the jumpless trajectory attain its maximum T^2 . This motivates a parameter estimation protocol based on the probabilistic preparation of the jumpless trajectory (which contains *all* the information about ω): ν successful preparations of the jumpless trajectory herald the estimation precision $\delta\omega = 1/\sqrt{\nu}T$, which attains the Heisenberg scaling. The drawback is that the success probability $P_\otimes(T) = 2/(e^{\gamma T} + 1)$ for each preparation decreases with increasing T .

For deterministic parameter estimation, we should take into account the occurrence probabilities of the quantum trajectories. The estimation precision of MQT is determined by

$$\mathbb{F}_\omega = \frac{\mathcal{F}_\omega[\bar{\rho}]}{\rho_{\uparrow\uparrow}e^{-\gamma T} + \rho_{\downarrow\downarrow}},$$

where $\mathcal{F}_\omega[\bar{\rho}] = 4T^2\rho_{\uparrow\uparrow}e^{-\gamma T}\rho_{\downarrow\downarrow}$ is the QFI of the conventional approach. For small $\rho_{\downarrow\downarrow}$, the enhancement of \mathbb{F}_ω relative to $\mathcal{F}_\omega[\bar{\rho}]$ could be very large when $\gamma T \gg 1$. In addition, MQT also shortens the total time cost: Once a quantum jump is detected, we should immediately stop the current measurement cycle (because the trajectory with a quantum jump has no QFI) and start the next measurement cycle. In this case, the average time cost for each measurement cycle is

$$T_{\text{ave}} = P_\otimes T + \int_0^T t_1 \text{Tr} \bar{\rho}_{t_1} dt_1 = \frac{\rho_{\uparrow\uparrow}}{\gamma}(1 - e^{-\gamma T}) + \rho_{\downarrow\downarrow} T, \quad (29)$$

which is shorter than T , especially when $\rho_{\downarrow\downarrow}$ is small. Since the total time cost of ν repeated measurement cycles is νT_{ave} , the estimation precision per unit time, i.e., the sensitivity $\delta\omega\sqrt{\nu T_{\text{ave}}} = 1/\sqrt{\mathbb{F}_\omega/T_{\text{ave}}}$ [cf. Eq. (27)], is determined by the

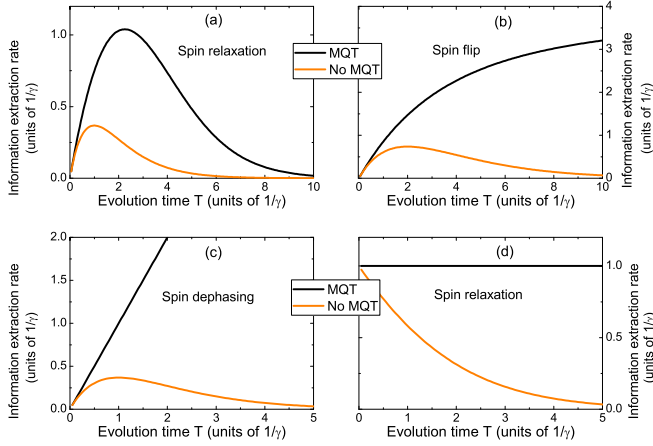


FIG. 3. Optimal information extraction rates (obtained by optimizing the initial states) for estimating (a)–(c) ω and (d) γ for different decoherence channels. Black lines are for MQT and orange lines for the conventional method.

information extraction rate

$$\frac{\mathbb{F}_\omega}{T_{\text{ave}}} \leq \frac{4\gamma T^2}{(\sqrt{e^{\gamma T} - 1} + \sqrt{\gamma T})^2} \xrightarrow{\gamma T \gg 1} 4\gamma T^2 e^{-\gamma T},$$

where the inequality is saturated at $\rho_{\downarrow\downarrow}/\rho_{\uparrow\uparrow} = \sqrt{(1 - e^{-\gamma T})/\gamma T e^{\gamma T}}$. For comparison, the information extracting rate of the conventional method is

$$\frac{\mathcal{F}_\omega[\bar{\rho}]}{T} \leq T e^{-\gamma T},$$

where the inequality is saturated at $\rho_{\downarrow\downarrow} = \rho_{\uparrow\uparrow} = 1/2$. Therefore, MQT enhances the long-time information extraction rate by a factor $4\gamma T$, although both \mathbb{F}_ω and $\mathcal{F}_\omega[\bar{\rho}]$ exhibit the same exponential decay, as shown in Fig. 3(a).

For the spin-flip channel, the jumpless trajectory [Eq. (22)] contains the QFI

$$\mathcal{F}_\omega[\rho_\emptyset] = 4T^2 \rho_{\uparrow\uparrow} \rho_{\downarrow\downarrow}$$

that attains the Heisenberg scaling with respect to T , while the trajectory with n quantum jumps at t_1, \dots, t_n [Eq. (23)] contains the QFI

$$\mathcal{F}_\omega[\rho_{t_1 \dots t_n}] = 4 \left(\int_0^T s(t) dt \right)^2 \rho_{\uparrow\uparrow} \rho_{\downarrow\downarrow},$$

where $s(t)$ starts from +1 at $t = 0$ and reverses its sign at t_1, \dots, t_n . Physically, every quantum jump reverses the direction of the phase accumulation [manifested as the sign reversal of $s(t)$] and $\int_0^T s(t) dt$ is the net phase accumulation time. For example, we consider the trajectory with a single quantum jump at t_1 . Starting from an initial state $a|\uparrow\rangle + b|\downarrow\rangle$, the quantum probe first evolves as $a|\uparrow\rangle + e^{i\omega t_1} b|\downarrow\rangle$ and then undergoes a spin flip into the state $a|\downarrow\rangle + e^{i\omega t_1} b|\uparrow\rangle$ and then evolve into the final state $a|\downarrow\rangle + e^{-i\omega(T-t_1)} e^{i\omega t_1} b|\uparrow\rangle$, so its net phase accumulation time is $t_1 - (T - t_1)$, which coincides with $\int_0^T s(t) dt$.

Here the Heisenberg scaling of $\mathcal{F}_\omega[\rho_\emptyset]$ again motivates a probabilistic parameter estimation protocol based on preparing the jumpless trajectory: ν successful preparations with

evolution time T and $\rho_{\uparrow\uparrow} = \rho_{\downarrow\downarrow} = 1/2$ herald the estimation precision $\delta\omega = 1/\sqrt{\nu T}$, which attains the Heisenberg scaling with respect to T . The drawback is that the success probability $P_\emptyset(T) = e^{-\gamma T/4}$ for each preparation decreases with increasing T , so this probabilistic protocol reduces the workload of data processing at the cost of reducing the fundamental estimation precision. For deterministic parameter estimation, we average the QFI of every trajectory over their occurrence probabilities to obtain

$$\frac{\mathbb{F}_\omega}{T} \xrightarrow{\gamma T \gg 1} \frac{16}{\gamma} \rho_{\uparrow\uparrow} \rho_{\downarrow\downarrow}.$$

For comparison, the information extraction rate of the conventional method is (for $\omega \gg \gamma$)

$$\frac{\mathcal{F}_\omega[\bar{\rho}]}{T} \approx 4T \rho_{\uparrow\uparrow} \rho_{\downarrow\downarrow} e^{-\gamma T/2}.$$

Thus MQT avoids the long-time exponential decay of the sensitivity (i.e., precision per unit time), as shown in Fig. 3(b). Physically, the jumpless trajectory has a negligible occurrence probability, so the long-time linear scaling $\mathbb{F}_\omega = \bar{\mathcal{F}}_\omega \propto T$ comes from the QFI of other trajectories: The random quantum jumps leads to random sign reversal of $s(t)$, so $[\int_0^T s(t) dt]^2$ and hence the QFI of each trajectory increase linearly with T on average, similar to a random walk. Monitoring quantum trajectories gives access to this trajectory-resolved QFI, as opposed to the ensemble QFI $\mathcal{F}_\omega[\bar{\rho}]$ from the conventional method.

When we take into account the finite interval Δ between successive syndrome measurements in QEC-based MQT for the spin-flip channel, we obtain

$$\begin{aligned} \mathbb{F}_\omega \approx & \frac{32\rho_{\uparrow\uparrow}\rho_{\downarrow\downarrow}}{\gamma^2} e^{-\gamma T/4} e^{2\zeta} \left[(1 - \zeta e^{-\zeta})^N + (1 + \zeta e^{-\zeta})^N \right. \\ & \left. \times \left(\frac{\gamma T}{2} e^{-\zeta} - 1 \right) \right] \end{aligned} \quad (30)$$

under the condition $1/\Delta \gg \omega \gg \gamma$ and $\gamma T \ll 1/\gamma \Delta$, where $\zeta \equiv \gamma \Delta/4$ and $N \equiv T/\Delta$ is the total number of syndrome measurements during the interval T . When the syndrome measurements are much faster than the decoherence ($\zeta \ll 1$), \mathbb{F}_ω approaches the ideal results in Table I. When each syndrome measurement is imperfect, we can combine several adjacent imperfect syndrome measurements into a composite measurement to suppress the measurement error exponentially.

Finally, we turn to the spin-dephasing channel. Interestingly, each quantum jump merely flips the phase between $|\uparrow\rangle$ and $|\downarrow\rangle$ without affecting the phase accumulation [Eq. (25)], so every quantum trajectory contain the same QFI

$$\mathbb{F}_\omega = \mathcal{F}_\omega[\rho_\emptyset] = \mathcal{F}_\omega[\rho_{t_1 \dots t_n}] = 4T^2 \rho_{\uparrow\uparrow} \rho_{\downarrow\downarrow}, \quad (31)$$

in contrast to the conventional method

$$\mathcal{F}_\omega[\bar{\rho}] = 4T^2 \rho_{\uparrow\uparrow} \rho_{\downarrow\downarrow} e^{-\gamma T}.$$

So MQT can restore the Heisenberg scaling of the estimation precision, as shown in Fig. 3(c). Unfortunately, QEC-based MQT for the dephasing channel of a single spin 1/2 is not possible, so direct measurement over the environment is necessary. For multiple qubits, the key to the recovery of the

Heisenberg scaling for estimating ω is $[\mathcal{J}, \mathcal{L}_0] = 0$ and the preservation of the QFI under the quantum jump \mathcal{J} [see the discussions after Eq. (18)]. When this condition is satisfied, QEC-based MQT can be used to recover the Heisenberg scaling (see Appendix B for an example).

C. Estimation of γ

For the spin-relaxation channel, the estimation precision of MQT is determined by $\mathbb{F}_\gamma \approx \rho_{\uparrow\uparrow}/\gamma^2$ at $\gamma T \gg 1$. By contrast, the estimation precision of the conventional method is determined by $\mathcal{F}_\gamma[\bar{\rho}] \approx T^2 \rho_{\uparrow\uparrow} e^{-\gamma T}$ at $\gamma T \gg 1$. Thus MQT avoids the exponential loss of the QFI in the conventional method. In addition, it also shortens the total time cost from T to T_{ave} [Eq. (29)]. The information extraction rate, which determines the sensitivity $\delta\gamma \sqrt{\nu T_{\text{ave}}} = 1/\sqrt{\mathbb{F}_\gamma/T_{\text{ave}}}$, is

$$\frac{\mathbb{F}_\gamma}{T_{\text{ave}}} \leq \frac{1}{\gamma}, \quad (32)$$

where the inequality is saturated at $\rho_{\downarrow\downarrow} = 0$. The information extracting rate of the conventional method is

$$\frac{\mathcal{F}_\gamma[\bar{\rho}]}{T} \leq \frac{T}{e^{\gamma T} - 1}, \quad (33)$$

where the inequality is saturated at $\rho_{\uparrow\downarrow} = \rho_{\downarrow\downarrow} = 0$. Therefore, MQT avoids the long-time exponential loss of the sensitivity, as shown in Fig. 3(d).

For the spin-flip channel, the information about γ is entirely the CFI in the timings of the quantum jumps: $\mathbb{F}_\gamma = F_\gamma = T/4\gamma$. The information extraction rate from the MQT is

$$\frac{\mathbb{F}_\gamma}{T} = \frac{1}{4\gamma}. \quad (34)$$

The information extraction rate of the conventional method is

$$\frac{\mathcal{F}_\gamma[\bar{\rho}]}{T} \leq \frac{T}{4(e^{\gamma T} - 1)}, \quad (35)$$

where ρ_{++} and ρ_{--} are the populations of $|\pm\rangle \equiv (|\uparrow\rangle \pm |\downarrow\rangle)/\sqrt{2}$ in the initial state ρ_0 and the inequality is saturated at $|\rho_{+-}|^2 = \rho_{++}\rho_{--}$ and $\rho_{++} = \rho_{--} = 1/2$. Equation (35) is also the ultimate precision bound [112] for adaptive estimation of the dephasing rate without MQT. Comparing Eq. (34) to Eq. (35), we see that MQT avoids the long-time exponential loss of the sensitivity. At $\omega = 0$, including the finite interval Δ between successive syndrome measurements in QEC-based MQT for the spin-flip channel amounts to a multiplicative factor $4\zeta/(e^{4\zeta} - 1)$ (with $\zeta \equiv \gamma\Delta/4$ and $N \equiv T/\Delta$) to \mathbb{F}_γ . When $\zeta \ll 1$, \mathbb{F}_γ approaches the ideal results in Table I. For the spin-dephasing channel, we obtain exactly the same results, with $|\uparrow\rangle$ ($|\downarrow\rangle$) playing the role of $|+\rangle$ ($|-\rangle$).

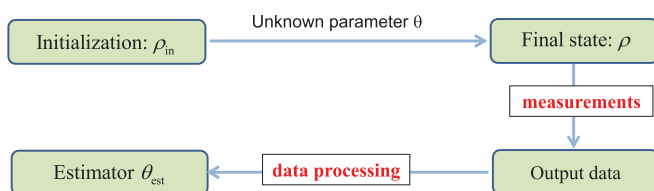


FIG. 4. Typical framework of quantum parameter estimation.

IV. CONCLUSION

Quantum-enhanced parameter estimation has widespread applications in many fields. An important issue is to protect the estimation precision against the noise-induced decoherence. For this purpose, we have developed a general theoretical framework for improving the precision of parameter estimation by monitoring the noise-induced quantum trajectories of the quantum probe and further establish its connection to the purification-based approach to quantum parameter estimation [61]. For Markovian environment, we provide a superoperator approach to determining the fundamental bounds on the estimation precision. This approach may provide exact analytical expressions for some simple models. Monitoring quantum trajectories can be achieved in two ways: (i) Any quantum trajectories can be monitored by directly monitoring the environment, which is experimentally challenging for realistic noises, and (ii) certain quantum trajectories can also be monitored by frequently measuring the quantum probe (without monitoring the environment) via ancilla-assisted encoding and error detection, as used in quantum error correction. This QEC-based MQT can be achieved in any experimental platform where QEC has been demonstrated, such as the nitrogen-vacancy center [26,81,82], superconducting qubits [83,84], and trapped ions [85–87]. It also establishes an interesting connection between MQT and the metrology protocols based on full QEC [21–28]. We apply MQT to the estimation of the level splitting ω and the decoherence rate γ of a spin 1/2 under three decoherence channels: spin relaxation, spin flip, and spin dephasing. We find that it can significantly improve the precision for estimating ω under the spin-relaxation channel, avoid the exponential loss of the precision for estimating γ (estimating ω) under all the decoherence channels (under the spin-flip channel), and recover the Heisenberg scaling for estimating ω under the spin-dephasing channel.

ACKNOWLEDGMENTS

This work was supported by the NSFC (Grants No. 11774021, No. 11704308, No. 11604261, and No. 11547166) and the NSFC program for Scientific Research Center (Grant No. U1530401).

APPENDIX A: FRAMEWORK OF QUANTUM PARAMETER ESTIMATION

Here we provide a self-contained introduction to the typical framework and important concepts in quantum parameter estimation. A typical (nonadaptive) parameter estimation protocol using a quantum probe to estimate an unknown real parameter θ consists of three steps (Fig. 4).

(1) The quantum probe starts from an initial state ρ_{in} and undergoes certain θ -dependent evolution into a final state ρ that depends on θ . This step imprints the information about θ into the final state ρ . The information contained in ρ is quantified by the quantum Fisher information \mathcal{F} .

(2) The quantum probe undergoes a measurement, which produces an outcome according to certain probability distribution. In this step, the quantum Fisher information \mathcal{F} contained in ρ is transferred into the classical information in

the measurement outcome. The information contained in each outcome is quantified by the classical Fisher information F , which obeys

$$F \leq \mathcal{F}. \quad (\text{A1})$$

(3) Steps 1 and 2 are repeated ν times and the ν outcomes are processed to yield an estimator θ_{est} to the unknown parameter θ . In this step, the total CFI νF contained in the ν outcomes is converted to the estimation precision, as quantified by the statistical error of the estimator

$$\delta\theta \equiv \sqrt{\langle (\theta_{\text{est}} - \theta)^2 \rangle}, \quad (\text{A2})$$

where $\langle \dots \rangle$ denotes the average over many estimators obtained by repeating steps 1–3 many times. For unbiased estimators obeying $\langle \theta_{\text{est}} \rangle = \theta$, the precision $\delta\theta$ is fundamentally limited by the inequality

$$\delta\theta \geq \frac{1}{\sqrt{\nu F}} \Leftrightarrow (\delta\theta)^{-2} \leq \nu F, \quad (\text{A3})$$

known as the Cramér-Rao bound [88–90].

1. Quantum Fisher information

The amount of information about θ contained in a general θ -dependent quantum state ρ is quantified by its QFI [90]

$$\mathcal{F} \equiv \text{Tr } \rho L^2,$$

where L is the so-called symmetric logarithmic derivative operator. It is an Hermitian operator defined through [89]

$$\partial_\theta \rho = \frac{1}{2}(L\rho + \rho L).$$

The QFI is invariant under any θ -independent unitary transformations. For a pure state $\rho = |\Phi\rangle\langle\Phi|$, we have $L = 2\partial_\theta \rho$ and hence

$$\mathcal{F} = 4(\langle \partial_\theta \Phi | \partial_\theta \Phi \rangle - |\langle \Phi | \partial_\theta \Phi \rangle|^2). \quad (\text{A4})$$

For a general mixed state with the spectral decomposition $\rho = \sum_n p_n |\Phi_n\rangle\langle\Phi_n|$, its QFI is [113–116]

$$\begin{aligned} \mathcal{F}[\rho] &= \sum_n \frac{(\partial_\theta p_n)^2}{p_n} + \sum_n p_n \mathcal{F}[|\Phi_n\rangle] \\ &\quad - \sum_{m \neq n} \frac{8p_m p_n}{p_m + p_n} |\langle \Phi_m | \partial_\theta \Phi_n \rangle|^2, \end{aligned}$$

where $\{p_n\}$ are *nonzero* eigenvalues of ρ , $\{|\Phi_n\rangle\}$ are the corresponding orthonormalized eigenstates, and $\mathcal{F}[|\Phi_n\rangle]$ is the QFI of the pure state $|\Phi_n\rangle$ [see Eq. (A4)]. For a two-level system, its density matrix can always be expressed in terms of the Pauli matrices $\boldsymbol{\sigma}$ as $\rho = (1/2)(1 + \boldsymbol{\sigma} \cdot \mathbf{n})$, where $\mathbf{n} \equiv \text{Tr } \boldsymbol{\sigma} \rho$ is the Bloch vector. The QFI for such a state is [16,117,118]

$$\mathcal{F} = |\partial_\theta \mathbf{n}|^2 + \frac{(\mathbf{n} \cdot \partial_\theta \mathbf{n})^2}{1 - |\mathbf{n}|^2},$$

where the second term is absent when $|\mathbf{n}| = 1$, i.e., when ρ is a pure state. When $\rho = \rho^{(1)} \otimes \dots \otimes \rho^{(N)}$ is the direct product state of N quantum probes, its QFI is additive: $\mathcal{F} = \sum_{n=1}^N \mathcal{F}[\rho^{(n)}]$.

The importance of the QFI for parameter estimation is manifested in the inequalities (A1) and (A3). Namely, given ρ

and hence \mathcal{F} , the precision of any unbiased estimator from ν repetitions of any measurement is limited by the inequality

$$\delta\theta \geq \frac{1}{\sqrt{\nu \mathcal{F}}}, \quad (\text{A5})$$

known as the quantum Cramér-Rao bound [89,90]. Saturating this bound requires saturating Eqs. (A1) and (A3) simultaneously, i.e., using optimal measurements to convert all the QFI into the CFI and using optimal unbiased estimators to convert all the CFI into the precision of the estimator.

2. Classical Fisher information and optimal measurements

A general measurement with discrete outcomes $\{u\}$ is described by the positive-operator-valued measure elements $\{M_u\}$ satisfying the completeness relation $\sum_u M_u^\dagger M_u = 1$. Given a quantum state ρ , it yields an outcome u according to the probability distribution $P(u|\theta) \equiv \text{Tr } M_u \rho M_u^\dagger$ that depends on θ . The amount of information about θ contained in each outcome is quantified by the CFI [88]

$$F \equiv \sum_u P(u|\theta) \left(\frac{\partial \ln P(u|\theta)}{\partial \theta} \right)^2. \quad (\text{A6})$$

For continuous outcomes, we only need to replace \sum_u by $\int du$ everywhere. The inequality (A1) expresses the simple fact that no new information about θ can be generated in the measurement process: Those measurements that convert all (part) of the QFI into the CFI are called optimal (nonoptimal). Given ρ , the optimal measurement is *not* unique. The projective measurement of the symmetric logarithmic derivative operator L has been identified [90] as an optimal measurement.

3. Optimal unbiased estimators

Given the measurement distribution $P(u|\theta)$ and hence the CFI F of each outcome, the precision $\delta\theta$ of any unbiased estimator $\theta_{\text{est}}(\mathbf{u})$ constructed from the outcomes $\mathbf{u} \equiv (u_1, \dots, u_\nu)$ of ν repeated measurements is limited by the Cramér-Rao bound (A3), which expresses the simple fact that no new information about θ can be generated in the data processing: Optimal (nonoptimal) unbiased estimators convert all (part) of the CFI into the useful information $(\delta\theta)^{-2}$ quantified by the precision $\delta\theta$. In the limit of large ν , two kinds of estimators are known to be unbiased and optimal, the maximum likelihood estimator and the Bayesian estimator [88], as we introduce now.

Before any measurements, our prior knowledge about the unknown parameter θ is quantified by a certain probability distribution $P_0(\theta)$, e.g., a δ -like distribution corresponds to knowing θ exactly, a flat distribution corresponds to completely no knowledge about θ , and a Gaussian distribution $P_0(\theta) \propto e^{-(\theta-\theta_0)^2/2\sigma_0^2}$ corresponds to knowing θ to be θ_0 with a typical uncertainty σ_0 .

Upon getting the first outcome u_1 , our knowledge about θ is immediately refined from $P_0(\theta)$ to

$$P_{u_1}(\theta) = \frac{P_0(\theta)P(u_1|\theta)}{\mathcal{N}(u_1)}$$

according to the Bayesian rule [119], where $\mathcal{N}(u_1) \equiv \int d\theta P_0(\theta)P(u_1|\theta)$ is a normalization factor ensuring $P_{u_1}(\theta)$ is

normalized to unity: $\int P_{u_1}(\theta)d\theta = 1$. Here $P_{u_1}(\theta)$ is the *posterior* probability distribution of θ conditioned on the outcome of the measurement being u_1 : Its parametric dependence on u_1 means that different measurement outcomes lead to different refinement of knowledge about θ .

Upon getting the second outcome u_2 , our knowledge is immediately refined from $P_{u_1}(\theta)$ to

$$P_{u_1 u_2}(\theta) = \frac{P_0(\theta)P(u_1|\theta)P(u_2|\theta)}{\mathcal{N}(u_1, u_2)},$$

where $\mathcal{N}(u_1, u_2) = \int P_0(\theta)P(u_1|\theta)P(u_2|\theta)d\theta$ is a normalization factor for the posterior distribution $P_{u_1 u_2}(\theta)$. If we omit the trivial normalization factors, then the measurement-induced knowledge refinement becomes

$$P_0(\theta) \xrightarrow{u_1} P_0(\theta)P(u_1|\theta) \xrightarrow{u_2} P_0(\theta)P(u_1|\theta)P(u_2|\theta) \xrightarrow{u_3} \dots$$

Upon getting ν outcomes $\mathbf{u} \equiv (u_1, \dots, u_\nu)$, our knowledge about θ is quantified by the posterior distribution

$$P_{\mathbf{u}}(\theta) \sim P_0(\theta)P(\mathbf{u}|\theta)$$

up to a trivial normalization factor, where $P(\mathbf{u}|\theta) = P(u_1|\theta) \cdots P(u_\nu|\theta)$ is the probability for getting the outcome \mathbf{u} . The posterior distribution $P_{\mathbf{u}}(\theta)$ completely describe our state of knowledge about θ . Nevertheless, sometimes a single number, i.e., an unbiased estimator, is required as the best guess to θ . There are two well-known estimators: The maximum likelihood estimator [88]

$$\theta_M(\mathbf{u}) \equiv \arg \max P_{\mathbf{u}}(\theta) \quad (\text{A7})$$

is the peak position of $P_{\mathbf{u}}(\theta)$ as a function of θ , while the Bayesian estimator [88]

$$\theta_B(\mathbf{u}) \equiv \int \theta P_{\mathbf{u}}(\theta) d\theta \quad (\text{A8})$$

is the average of θ . For large ν , both estimators are unbiased and optimal: $\langle \theta_\alpha \rangle = \theta$ and $\delta\theta_\alpha = 1/\sqrt{\nu F(\theta)}$, where $\alpha = M$ or B , $\langle \cdots \rangle$ denotes the average over a large number of estimators obtained by repeating the ν -outcome estimation scheme many times, and $\delta\theta_\alpha$ is defined as Eq. (A2) or

$$\delta\theta_\alpha = \sqrt{\int [\theta - \theta_\alpha(\mathbf{u})]^2 P_{\mathbf{u}}(\theta) d\theta}. \quad (\text{A9})$$

APPENDIX B: MONITORING DEPHASING OF LOGICAL QUBITS

We consider an odd number m of spins $1/2$ and each spin $1/2$ is subjected to an independent spin-dephasing channel. The quantum jump operator S_z of the dephasing channel leads to random transitions between the two eigenstates $|\pm\rangle \equiv (|\uparrow\rangle \pm |\downarrow\rangle)/\sqrt{2}$ of σ_x during the evolution. We define the $(m-1)$ -component syndrome operator $\Sigma = (\sigma_x^{(1)}\sigma_x^{(2)}, \dots, \sigma_x^{(m-1)}\sigma_x^{(m)})$, where $\sigma_x^{(i)}$ is the Pauli matrix for the i th spin $1/2$. The code subspace as spanned by [21,24]

$$|\uparrow\rangle \equiv \frac{|+\rangle^{\otimes m} + |-\rangle^{\otimes m}}{\sqrt{2}}, \quad |\downarrow\rangle \equiv \frac{|+\rangle^{\otimes m} - |-\rangle^{\otimes m}}{\sqrt{2}}$$

is an eigensubspace of Σ with eigenvalue $+1$ for every component of Σ . This allows us to monitor the simultaneous quantum jump of at most $(m-1)/2$ qubits [21,24], e.g., the quantum jump of the i th spin $1/2$ switches the sign of the $(i-1)$ th and the i th component of Σ , while leaving other components of Σ intact. When the Hamiltonian commutes with the syndrome operator, monitoring the quantum jump does not affect the Hamiltonian evolution. When the Hamiltonian further commutes with all the quantum jump operators $S_z^{(1)}, \dots, S_z^{(m)}$, the quantum jump does not affect the Hamiltonian evolution. In this case, MQT can fully recover the estimation precision in the noiseless case.

As an example, we consider $H = (\omega/2)\bar{\sigma}_z$, where $\bar{\sigma}_z \equiv \sigma_z^{\otimes m}$ maps $|\uparrow\rangle$ to $|\uparrow\rangle$ and $|\downarrow\rangle$ to $-|\downarrow\rangle$. This Hamiltonian commutes with the syndrome operator and all the quantum jump operators. The initial state $|\psi_0\rangle = (|\uparrow\rangle + |\downarrow\rangle)/\sqrt{2}$ lies inside the code subspace. In the absence of quantum jumps, the final state is $|\psi\rangle = (|\uparrow\rangle + e^{i\omega T}|\downarrow\rangle)/\sqrt{2}$, whose QFI $\mathcal{F}_\omega[|\psi\rangle] = T^2$ attains the Heisenberg scaling with respect to the time cost T . By frequently measuring the syndrome operator, we can track the simultaneous phase flips of at most $(m-1)/2$ qubits. Since the phase flips commute with H , they always map $|\uparrow\rangle$ ($|\downarrow\rangle$) to another eigenstate of H with the *same* eigenvalue, thus all the detectable quantum jumps do not cause the loss of the QFI. For example, a quantum jump of the k th qubit at time t maps the m -qubit state $(|\uparrow\rangle + e^{i\omega t}|\downarrow\rangle)/\sqrt{2}$ to $(\sigma_z^{(k)}|\uparrow\rangle + e^{i\omega t}\sigma_z^{(k)}|\downarrow\rangle)/\sqrt{2}$, where $\sigma_z^{(k)}|\uparrow\rangle$ ($\sigma_z^{(k)}|\downarrow\rangle$) is still an eigenstate of $\bar{\sigma}_z$ with the same eigenvalue $+1$ (-1). Afterward, the evolution under $H = (\omega/2)\bar{\sigma}_z$ leads to the final state $(\sigma_z^{(k)}|\uparrow\rangle + e^{i\omega T}\sigma_z^{(k)}|\downarrow\rangle)/\sqrt{2}$, which contains the same QFI as the jumpless state. Therefore, MQT allows us to continuously track the quantum trajectory and hence recover the Heisenberg scaling of the estimation precision without error correction, as long as in between two rounds of syndrome measurements the number of phase-flipped qubits does not exceed $(m-1)/2$. By contrast, when the quantum trajectories are not monitored, the QFI of the nonselective final state would decay to zero on timescales much greater than the single-qubit decoherence time.

The results above are consistent with the conclusion of Refs. [68,69] since the Hamiltonian $H \propto \bar{\sigma}_z = \sigma_z^{\otimes m}$ lies outside the Lindblad span of all the decoherence channels. The results above can also be generalized to N logical qubits, where each logical qubit is composed of m qubits through the m -qubit phase-flip code and is driven by the Hamiltonian $(\omega/2)\bar{\sigma}_z$. Starting from the initial state $(|\uparrow\rangle^{\otimes N} + |\downarrow\rangle^{\otimes N})/\sqrt{2}$, all the detectable quantum trajectories contain the same QFI $N^2 T^2$, which gives the Heisenberg scaling for the estimation precision about ω .

APPENDIX C: ESTIMATION PRECISION FOR SPIN-FLIP CHANNEL

1. Ideal continuous monitoring

For ideal continuous monitoring of the quantum jump (i.e., spin flip), the normalized quantum trajectory with n quantum

jumps at t_1, \dots, t_n has the QFI

$$\mathcal{F}_\omega[\rho_{t_1 \dots t_n}] = \begin{cases} 4|\rho_{\uparrow\downarrow}|^2(T - 2t_1 + 2t_2 - \dots - 2t_{2k+1})^2 & (n = 2k + 1) \\ 4|\rho_{\uparrow\downarrow}|^2(T + 2t_1 - 2t_2 + \dots - 2t_{2k})^2 & (n = 2k), \end{cases}$$

with occurrence probability density $p_{t_1 \dots t_n} = (\gamma/4)^n e^{-\gamma T/4}$. For $n = 0$, they reduce to the QFI and the occurrence probability of the jumpless trajectory. The trajectory-averaged QFI follows by straightforward calculation:

$$\bar{\mathcal{F}}_\omega = 4T^2 |\rho_{\uparrow\downarrow}|^2 e^{-\gamma T/4} \sum_{k=0}^{\infty} \frac{(\gamma T/4)^{2k}}{(2k+1)!} \left(1 + \frac{\gamma T/4}{2k+3}\right).$$

The sum $\sum_{k=0}^{\infty}(\dots)$ is equal to $(xe^x - \sinh x)/x^2$ with $x \equiv \gamma T/4$, so we obtain the $\bar{\mathcal{F}}_\omega$ listed in Table I. Since $p_{t_1 \dots t_n}$ is independent of ω and the timings $\{t_1, \dots, t_n\}$ of the quantum jumps, Eq. (18) gives $F_\omega = 0$ and

$$F_\gamma = \frac{(\partial_\gamma P_\emptyset)^2}{P_\emptyset} + \sum_{n=1}^{\infty} \frac{(\partial_\gamma P_n)^2}{P_n} = \frac{T}{4\gamma}, \quad (\text{C1})$$

where

$$P_n \equiv \int_0^T dt_n \dots \int_0^{t_2} dt_1 p_{t_1 \dots t_n} = \frac{(\gamma T/4)^n}{n!} e^{-\gamma T/4}$$

is the probability for n quantum jumps during $[0, T]$.

2. Realistic QEC-based monitoring

When we use QEC-based MQT with the syndrome operator $\Sigma \equiv \sigma_z \sigma_z^{(a)}$ with eigenvalues ± 1 (see Sec. II E), the interval Δ between successive syndrome measurements is finite. The total evolution interval $[0, T]$ is divided into $N = T/\Delta \gg 1$ segments of length Δ sandwiched by N syndrome measurements at $t = \Delta, 2\Delta, \dots, N\Delta$. At $t = 0$, the initial state of the spin 1/2 and the ancilla is an eigenstate of the syndrome operator with eigenvalue $\lambda_0 \equiv +1$. For clarity we use λ_k ($=+1$ or -1) to denote the outcome of the k th syndrome measurement, where $k = 1, 2, \dots, N$. If the k th syndrome measurement reports a sign switch, i.e., $\lambda_k = -\lambda_{k-1}$, then the spin 1/2 undergoes an odd number of quantum jumps during $[(k-1)\Delta, k\Delta]$; otherwise (i.e., $\lambda_k = \lambda_{k-1}$) the spin 1/2 undergoes an even number of quantum jumps during $[(k-1)\Delta, k\Delta]$. If $\gamma\Delta \ll 1$, then the possibility of multiple quantum jumps between neighboring syndrome measurement is exponentially small, so the syndrome measurements can resolve well individual quantum jumps. Otherwise, the syndrome measurements only give little information about the quantum jumps.

First, we derive the evolution of the quantum trajectories between the $(k-1)$ th and the k th syndrome measurements. Suppose the previous syndrome measurements give the outcomes $\lambda_1, \dots, \lambda_{k-1}$ and the unnormalized quantum trajectory $\tilde{\rho}$ immediately after the $(k-1)$ th syndrome measurement is

$$\tilde{\rho} \equiv \begin{bmatrix} \tilde{\rho}_{\uparrow\uparrow} & \tilde{\rho}_{\uparrow\downarrow} \\ \tilde{\rho}_{\uparrow\downarrow}^* & \tilde{\rho}_{\downarrow\downarrow} \end{bmatrix},$$

which is an eigenstate of Σ with eigenvalue λ_{k-1} . The *nonselective* evolution during $[(k-1)\Delta, k\Delta]$ gives the nonselective

final state

$$e^{\mathcal{L}\Delta} \tilde{\rho} = \mathcal{M}_+ \tilde{\rho} + \mathcal{M}_- \tilde{\rho},$$

where $\mathcal{L}\rho = -i[H, \rho] + \gamma\mathcal{D}[S_x]\rho$ and \mathcal{M}_\pm are superoperators

$$\mathcal{M}_+ \tilde{\rho} \equiv e^{-\zeta} \begin{bmatrix} \tilde{\rho}_{\uparrow\uparrow} \cosh \zeta & \tilde{\rho}_{\uparrow\downarrow} f(\Delta) \\ \tilde{\rho}_{\uparrow\downarrow}^* f^*(\Delta) & \tilde{\rho}_{\downarrow\downarrow} \cosh \zeta \end{bmatrix},$$

$$\mathcal{M}_- \tilde{\rho} \equiv e^{-\zeta} \begin{bmatrix} \tilde{\rho}_{\downarrow\downarrow} \sinh \zeta & \tilde{\rho}_{\uparrow\downarrow}^* g(\Delta) \\ \tilde{\rho}_{\uparrow\downarrow} g(\Delta) & \tilde{\rho}_{\uparrow\uparrow} \sinh \zeta \end{bmatrix},$$

with $\zeta \equiv \gamma\Delta/4$, $f(\Delta) \equiv \cos(w\Delta) - i(\omega/w)\sin(w\Delta)$, $g(\Delta) \equiv \gamma \sin(w\Delta)/4w$, and $w \equiv \sqrt{\omega^2 - (\gamma/4)^2}$. Since each quantum jump leads to the exchanges $|\uparrow\rangle \leftrightarrow |\downarrow\rangle$ and hence $\tilde{\rho}_{\uparrow\uparrow} \leftrightarrow \tilde{\rho}_{\downarrow\downarrow}$ and $\tilde{\rho}_{\uparrow\downarrow} \leftrightarrow \tilde{\rho}_{\downarrow\uparrow}$, we identify $\tilde{\rho}_+ \equiv \mathcal{M}_+ \tilde{\rho}$ ($\tilde{\rho}_- \equiv \mathcal{M}_- \tilde{\rho}$) as the unnormalized quantum trajectory containing an even (odd) number of quantum jumps during $[(k-1)\Delta, k\Delta]$. In other words, the unnormalized quantum trajectory at $t = k\Delta$ is $\tilde{\rho}_-$ if the k th syndrome measurement reports a sign switch or $\tilde{\rho}_+$ otherwise. Their occurrence probabilities are $\text{Tr} \tilde{\rho}_\pm = [(1 \pm e^{-2\zeta})/2] \text{Tr} \tilde{\rho}$, so the nonselective evolution is trace preserving: $\text{Tr} \mathcal{M}_+ \tilde{\rho} + \text{Tr} \mathcal{M}_- \tilde{\rho} = \text{Tr} \tilde{\rho}$. When $\text{Tr} \tilde{\rho} = 1$, the occurrence probabilities of $\tilde{\rho}_\pm$ are $p \equiv (1 + e^{-2\zeta})/2$ and $1 - p$, respectively.

This single-step evolution can be iterated N times to yield the quantum trajectories at $t = T$. Specifically, if only the syndrome measurements at $t = k_1\Delta, \dots, k_m\Delta$ report sign switches, then the unnormalized quantum trajectory at $t = T$ is

$$\tilde{\rho}_{k_1 \dots k_m} = \mathcal{M}_+^{N-k_m-1} \mathcal{M}_- \mathcal{M}_+^{k_m-k_{m-1}-1} \dots \mathcal{M}_- \mathcal{M}_+^{k_2-k_1-1} \\ \times \mathcal{M}_- \mathcal{M}_+^{k_1-1} \rho_0$$

and its occurrence probability

$$P_{k_1 \dots k_m} \equiv \text{Tr} \tilde{\rho}_{k_1 \dots k_m} = p^{N-m} (1-p)^m$$

is independent of k_1, \dots, k_m . Since p is independent of ω , the CFI about ω vanishes, $F_\omega = 0$, and the CFI about γ follows from Eq. (18) as

$$F_\gamma = \sum_{m=0}^N \sum_{\{k_1, \dots, k_m\}} \frac{(\partial_\gamma P_{k_1 \dots k_m})^2}{P_{k_1 \dots k_m}} = \sum_{m=0}^N \frac{(\partial_\gamma P_m)^2}{P_m} = \frac{T}{4\gamma} \frac{4\zeta}{e^{4\zeta} - 1},$$

where $P_m \equiv \sum_{k_1 < k_2 < \dots < k_m} P_{k_1 \dots k_m} = C_N^m p^{N-m} (1-p)^m$ is the probability for m quantum jumps during $[0, T]$ and $C_N^m \equiv N!/m!(N-m)!$ is the binomial coefficient. Next we calculate the QFI in the normalized quantum trajectories: $\rho_{k_1 \dots k_m} \equiv \tilde{\rho}_{k_1 \dots k_m} / P_{k_1 \dots k_m}$.

When $\omega = 0$, we have $f(\Delta) = \cosh \zeta$, $g(\Delta) = \sinh \zeta$, and hence $\mathcal{M}_+\rho_0 = p\rho_0$ and $\mathcal{M}_-\rho_0 = (1-p)\sigma_x\rho_0\sigma_x$, so $\rho_{k_1\dots k_m} = \rho_0$ (for even m) or $\rho_{k_1\dots k_m} = \sigma_x\rho_0\sigma_x$ (for odd m) is independent of γ and hence gives zero-trajectory QFI about γ . In this case, the total information from MQT is $\mathbb{F}_\gamma = F_\gamma$.

When $\omega \neq 0$, to obtain explicit analytical expression, we assume $1/\Delta \gg \omega \gg \gamma$ and $\gamma T \ll 1/(\gamma\Delta)$, so $f(\Delta) \approx e^{-i\omega\Delta}$, $g(\Delta) \approx \zeta$, and hence

$$\rho_{k_1\dots k_m} = \begin{bmatrix} \rho_{\downarrow\downarrow} & a \\ a^* & \rho_{\uparrow\uparrow} \end{bmatrix} \quad (\text{for } m = 2n + 1),$$

$$\rho_{k_1\dots k_m} = \begin{bmatrix} \rho_{\uparrow\uparrow} & b \\ b^* & \rho_{\downarrow\downarrow} \end{bmatrix} \quad (\text{for } m = 2n),$$

where

$$a \equiv \frac{\rho_{\uparrow\downarrow}^* e^{-\gamma T/4}}{p^{N-2n-1}(1-p)^{2n+1}} \zeta^{2n+1} \exp \left[-i\omega\Delta \left(N + 1 + 2 \sum_{i=1}^{2n+1} (-1)^i k_i \right) \right],$$

$$b \equiv \frac{\rho_{\uparrow\downarrow} e^{-\gamma T/4}}{p^{N-2n}(1-p)^{2n}} \zeta^{2n} \exp \left[-i\omega\Delta \left(N + 2 \sum_{i=1}^{2n} (-1)^{i+1} k_i \right) \right].$$

The trajectory QFI is

$$\mathcal{F}_\omega[\rho_{k_1\dots k_m}] = 4|\rho_{\uparrow\downarrow}|^2 \frac{\zeta^{2m} \Delta^2 e^{-\gamma T/2}}{[p^{N-m}(1-p)^m]^2} \begin{cases} (N - 2k_{2n+1} + 2k_{2n} - \dots - 2k_1 + 1)^2 & (m = 2n + 1) \\ (N - 2k_{2n} + 2k_{2n-1} - \dots + 2k_1)^2 & (m = 2n). \end{cases}$$

Averaging the trajectory-QFI over its occurrence probabilities gives

$$\bar{\mathcal{F}}_\omega \approx 4|\rho_{\uparrow\downarrow}|^2 e^{-\gamma T/4} \Delta^2 \sum_{n=0}^{\lfloor N/2 \rfloor} \left(N \frac{N(N-1)\dots(N-2n)}{(2n+1)!} (\zeta e^{-\zeta})^{2n} + \frac{(N+1)N\dots(N-2n-1)}{(2n+3)(2n+1)!} (\zeta e^{-\zeta})^{2n+1} \right),$$

where $\lfloor x \rfloor$ is the largest integer not greater than x and we have used $p^{N-m} \approx e^{-(N-m)\zeta}$ and $(1-p)^m \approx \zeta^m$. Performing the summation gives Eq. (30) of the main text.

-
- [1] V. Giovannetti, S. Lloyd, and L. Maccone, *Phys. Rev. Lett.* **96**, 010401 (2006).
- [2] C. L. Degen, F. Reinhard, and P. Cappellaro, *Rev. Mod. Phys.* **89**, 035002 (2017).
- [3] C. M. Caves, *Phys. Rev. D* **23**, 1693 (1981).
- [4] J. Aasi *et al.* (LIGO Scientific Collaboration), *Nat. Photon.* **7**, 613 (2013).
- [5] D. J. Wineland, J. J. Bollinger, W. M. Itano, F. L. Moore, and D. J. Heinzen, *Phys. Rev. A* **46**, R6797 (1992).
- [6] J. J. Bollinger, W. M. Itano, D. J. Wineland, and D. J. Heinzen, *Phys. Rev. A* **54**, R4649 (1996).
- [7] D. Budker and M. Romalis, *Nat. Phys.* **3**, 227 (2007).
- [8] L. Rondin, J.-P. Tetienne, T. Hingant, J.-F. Roch, P. Maletinsky, and V. Jacques, *Rep. Prog. Phys.* **77**, 056503 (2014).
- [9] J. P. Dowling, *Contemp. Phys.* **49**, 125 (2008).
- [10] J. Borregaard and A. S. Sørensen, *Phys. Rev. Lett.* **111**, 090801 (2013).
- [11] W. Yang, W.-L. Ma, and R.-B. Liu, *Rep. Prog. Phys.* **80**, 016001 (2017).
- [12] J. R. Maze, P. L. Stanwix, J. S. Hodges, S. Hong, J. M. Taylor, P. Cappellaro, L. Jiang, M. V. G. Dutt, E. Togan, A. S. Zibrov, A. Yacoby, R. L. Walsworth, and M. D. Lukin, *Nature (London)* **455**, 644 (2008).
- [13] J. M. Taylor, P. Cappellaro, L. Childress, L. Jiang, D. Budker, P. R. Hemmer, A. Yacoby, R. Walsworth, and M. D. Lukin, *Nat. Phys.* **4**, 810 (2008).
- [14] N. Zhao, J.-L. Hu, S.-W. Ho, J. T. K. Wan, and R.-B. Liu, *Nat. Nanotechnol.* **6**, 242 (2011).
- [15] J. Cai, F. Jelezko, M. B. Plenio, and A. Retzker, *New J. Phys.* **15**, 013020 (2013).
- [16] Y.-L. Li, X. Xiao, and Y. Yao, *Phys. Rev. A* **91**, 052105 (2015).
- [17] W. Yang, Z.-Y. Wang, and R.-B. Liu, *Front. Phys.* **6**, 2 (2011).
- [18] Y. Matsuzaki, S. C. Benjamin, and J. Fitzsimons, *Phys. Rev. A* **84**, 012103 (2011).
- [19] A. W. Chin, S. F. Huelga, and M. B. Plenio, *Phys. Rev. Lett.* **109**, 233601 (2012).
- [20] R. Chaves, J. B. Brask, M. Markiewicz, J. Kolodnyski, and A. Acin, *Phys. Rev. Lett.* **111**, 120401 (2013).
- [21] W. Dür, M. Skotiniotis, F. Fröwis, and B. Kraus, *Phys. Rev. Lett.* **112**, 080801 (2014).
- [22] E. M. Kessler, I. Lovchinsky, A. O. Sushkov, and M. D. Lukin, *Phys. Rev. Lett.* **112**, 150802 (2014).
- [23] G. Arrad, Y. Vinkler, D. Aharonov, and A. Retzker, *Phys. Rev. Lett.* **112**, 150801 (2014).
- [24] X.-M. Lu, S. Yu, and C. H. Oh, *Nat. Commun.* **6**, 7282 (2015).
- [25] D. A. Herrera-Martí, T. Gefen, D. Aharonov, N. Katz, and A. Retzker, *Phys. Rev. Lett.* **115**, 200501 (2015).
- [26] T. Unden, P. Balasubramanian, D. Louzon, Y. Vinkler, M. B. Plenio, M. Markham, D. Twitchen, A. Stacey, I. Lovchinsky, A. O. Sushkov, M. D. Lukin, A. Retzker, B. Naydenov, L. P. McGuinness, and F. Jelezko, *Phys. Rev. Lett.* **116**, 230502 (2016).

- [27] M. Bergmann and P. van Loock, *Phys. Rev. A* **94**, 012311 (2016).
- [28] Y. Matsuzaki and S. Benjamin, *Phys. Rev. A* **95**, 032303 (2017).
- [29] Q. Zheng, L. Ge, Y. Yao, and Q.-j. Zhi, *Phys. Rev. A* **91**, 033805 (2015).
- [30] M. Hirose and P. Cappellaro, *Nature (London)* **532**, 77 (2016).
- [31] J. Liu and H. Yuan, *Phys. Rev. A* **96**, 012117 (2017).
- [32] Y. Watanabe, T. Sagawa, and M. Ueda, *Phys. Rev. Lett.* **104**, 020401 (2010).
- [33] A. Laraoui, F. Dolde, C. Burk, F. Reinhard, J. Wrachtrup, and C. A. Meriles, *Nat. Commun.* **4**, 1651 (2013).
- [34] Q.-S. Tan, Y. Huang, X. Yin, L.-M. Kuang, and X. Wang, *Phys. Rev. A* **87**, 032102 (2013).
- [35] N. Zhao, J. Wrachtrup, and R.-B. Liu, *Phys. Rev. A* **90**, 032319 (2014).
- [36] N. Zhao and Z. Q. Yin, *Phys. Rev. A* **90**, 042118 (2014).
- [37] J. M. Boss, K. Chang, J. Armijo, K. Cujia, T. Rosskopf, J. R. Maze, and C. L. Degen, *Phys. Rev. Lett.* **116**, 197601 (2016).
- [38] W.-L. Ma and R.-B. Liu, *Phys. Rev. Appl.* **6**, 054012 (2016).
- [39] W.-L. Ma and R.-B. Liu, *Phys. Rev. Appl.* **6**, 024019 (2016).
- [40] F. Yan, S. Gustavsson, J. Bylander, X. Jin, F. Yoshihara, D. G. Cory, Y. Nakamura, T. P. Orlando, and W. D. Oliver, *Nat. Commun.* **4**, 2337 (2013).
- [41] M. Loretz, T. Rosskopf, and C. L. Degen, *Phys. Rev. Lett.* **110**, 017602 (2013).
- [42] J. E. Lang, R. B. Liu, and T. S. Monteiro, *Phys. Rev. X* **5**, 041016 (2015).
- [43] S. Kotler, N. Akerman, Y. Glickman, A. Keselman, and R. Ozeri, *Nature (London)* **473**, 61 (2011).
- [44] G. de Lange, D. Ristè, V. V. Dobrovitski, and R. Hanson, *Phys. Rev. Lett.* **106**, 080802 (2011).
- [45] G. de Lange, Z. H. Wang, D. Riste, V. V. Dobrovitski, and R. Hanson, *Science* **330**, 60 (2010).
- [46] G. A. Álvarez and D. Suter, *Phys. Rev. Lett.* **107**, 230501 (2011).
- [47] J. Medford, L. Cywiński, C. Barthel, C. M. Marcus, M. P. Hanson, and A. C. Gossard, *Phys. Rev. Lett.* **108**, 086802 (2012).
- [48] N. Bar-Gill, L. Pham, C. Belthangady, D. Le Sage, P. Cappellaro, J. Maze, M. Lukin, A. Yacoby, and R. Walsworth, *Nat. Commun.* **3**, 858 (2012).
- [49] J. T. Muhonen, J. P. Dehollain, A. Laucht, F. E. Hudson, R. Kalra, T. Sekiguchi, K. M. Itoh, D. N. Jamieson, J. C. McCallum, A. S. Dzurak, and A. Morello, *Nat. Nano* **9**, 986 (2014).
- [50] N. Zhao, J. Honert, B. Schmid, M. Klas, J. Isoya, M. Markham, D. Twitchen, F. Jelezko, R.-B. Liu, H. Fedder, and J. Wrachtrup, *Nat. Nano* **7**, 657 (2012).
- [51] S. Kolkowitz, Q. P. Unterreithmeier, S. D. Bennett, and M. D. Lukin, *Phys. Rev. Lett.* **109**, 137601 (2012).
- [52] T. H. Taminiu, J. J. T. Wagenaar, T. van der Sar, F. Jelezko, V. V. Dobrovitski, and R. Hanson, *Phys. Rev. Lett.* **109**, 137602 (2012).
- [53] P. London, J. Scheuer, J.-M. Cai, I. Schwarz, A. Retzker, M. B. Plenio, M. Katagiri, T. Teraji, S. Koizumi, J. Isoya, R. Fischer, L. P. McGuinness, B. Naydenov, and F. Jelezko, *Phys. Rev. Lett.* **111**, 067601 (2013).
- [54] T. Staudacher, F. Shi, S. Pezzagna, J. Meijer, J. Du, C. A. Meriles, F. Reinhard, and J. Wrachtrup, *Science* **339**, 561 (2013).
- [55] H. J. Mamin, M. Kim, M. H. Sherwood, C. T. Rettner, K. Ohno, D. D. Awschalom, and D. Rugar, *Science* **339**, 557 (2013).
- [56] F. Shi, X. Kong, P. Wang, F. Kong, N. Zhao, R.-B. Liu, and J. Du, *Nat. Phys.* **10**, 21 (2014).
- [57] X.-M. Lu, X. Wang, and C. P. Sun, *Phys. Rev. A* **82**, 042103 (2010).
- [58] K. Berrada, *Phys. Rev. A* **88**, 035806 (2013).
- [59] P. Sekatski, M. Skotiniotis, and W. Dür, *New J. Phys.* **18**, 073034 (2016).
- [60] Y.-S. Wang, C. Chen, and J.-H. An, *New J. Phys.* **19**, 113019 (2017).
- [61] A. Fujiwara and H. Imai, *J. Phys. A: Math. Theor.* **41**, 255304 (2008).
- [62] B. M. Escher, R. L. de Matos Filho, and L. Davidovich, *Nat. Phys.* **7**, 406 (2011).
- [63] R. Demkowicz-Dobrzanski, J. Kolodynski, and M. Guta, *Nat. Commun.* **3**, 1063 (2012).
- [64] B. M. Escher, L. Davidovich, N. Zagury, and R. L. de Matos Filho, *Phys. Rev. Lett.* **109**, 190404 (2012).
- [65] M. Jarzyna and R. Demkowicz-Dobrzański, *Phys. Rev. Lett.* **110**, 240405 (2013).
- [66] R. Demkowicz-Dobrzański and L. Maccone, *Phys. Rev. Lett.* **113**, 250801 (2014).
- [67] R. Demkowicz-Dobrzański, M. Jarzyna, and J. Kołodyński, in *Progress in Optics*, edited by E. Wolf (Elsevier, Amsterdam, 2015), Vol. 60, pp. 345–435.
- [68] R. Demkowicz-Dobrzański, J. Czajkowski, and P. Sekatski, *Phys. Rev. X* **7**, 041009 (2017).
- [69] S. Zhou, M. Zhang, J. Preskill, and L. Jiang, *Nat. Commun.* **9**, 78 (2018).
- [70] C. Catana and M. Guță, *Phys. Rev. A* **90**, 012330 (2014).
- [71] F. Albarelli, M. A. C. Rossi, M. G. A. Paris, and M. G. Genoni, *New J. Phys.* **19**, 123011 (2017).
- [72] F. Albarelli, M. A. C. Rossi, D. Tamascelli, and M. G. Genoni, *Quantum* **2**, 110 (2018).
- [73] S. Gammelmark and K. Mølmer, *Phys. Rev. A* **87**, 032115 (2013).
- [74] S. Gammelmark and K. Mølmer, *Phys. Rev. Lett.* **112**, 170401 (2014); S. A. Haine and S. S. Szigeti, *Phys. Rev. A* **92**, 032317 (2015).
- [75] M. G. Genoni, *Phys. Rev. A* **95**, 012116 (2017).
- [76] H. Yuan and C.-H. F. Fung, *Phys. Rev. A* **96**, 012310 (2017).
- [77] P. Sekatski, M. Skotiniotis, J. Kolodynski, and W. Dur, *Quantum* **1**, 27 (2017).
- [78] R. H. Hadfield, *Nat. Photon.* **3**, 696 (2009).
- [79] M. D. Eisaman, J. Fan, A. Migdall, and S. V. Polyakov, *Rev. Sci. Instrum.* **82**, 071101 (2011).
- [80] C. M. Natarajan, M. G. Tanner, and R. H. Hadfield, *Supercond. Sci. Technol.* **25**, 063001 (2012).
- [81] T. H. Taminiu, J. Cramer, T. van der Sar, V. V. Dobrovitski, and R. Hanson, *Nat. Nanotechnol.* **9**, 171 (2014).
- [82] G. Waldherr, Y. Wang, S. Zaiser, M. Jamali, T. Schulte-Herbrüggen, H. Abe, T. Ohshima, J. Isoya, J. Du, P. Neumann *et al.*, *Nature (London)* **506**, 204 (2014).

- [83] M. D. Reed, L. DiCarlo, S. E. Nigg, L. Sun, L. Frunzio, S. M. Girvin, and R. J. Schoelkopf, *Nature (London)* **482**, 382 (2012).
- [84] N. Ofek, A. Petrenko, R. Heeres, P. Reinhold, Z. Leghtas, B. Vlastakis, Y. Liu, L. Frunzio, S. Girvin, L. Jiang *et al.*, *Nature (London)* **536**, 441 (2016).
- [85] P. Schindler, J. T. Barreiro, T. Monz, V. Nebendahl, D. Nigg, M. Chwalla, M. Hennrich, and R. Blatt, *Science* **332**, 1059 (2011).
- [86] J. Chiaverini, D. Leibfried, T. Schaetz, M. D. Barrett, R. Blakestad, J. Britton, W. M. Itano, J. D. Jost, E. Knill, C. Langer *et al.*, *Nature (London)* **432**, 602 (2004).
- [87] F. Reiter, A. S. Sørensen, P. Zoller, and C. Muschik, *Nat. Commun.* **8**, 1822 (2017).
- [88] S. M. Kay, *Fundamentals of Statistical Signal Processing: Estimation Theory* (Prentice-Hall, Englewood Cliffs, 1993).
- [89] C. W. Helstrom, *Quantum Detection and Estimation Theory* (Academic, New York, 1976).
- [90] S. L. Braunstein and C. M. Caves, *Phys. Rev. Lett.* **72**, 3439 (1994).
- [91] C. M. Kropf, C. Gneiting, and A. Buchleitner, *Phys. Rev. X* **6**, 031023 (2016).
- [92] A. Smirne, J. Kołodzyński, S. F. Huelga, and R. Demkowicz-Dobrzański, *Phys. Rev. Lett.* **116**, 120801 (2016).
- [93] J. Combes, C. Ferrie, Z. Jiang, and C. M. Caves, *Phys. Rev. A* **89**, 052117 (2014).
- [94] C. Ferrie, *Phys. Rev. A* **90**, 014101 (2014).
- [95] S. Alipour and A. T. Rezakhani, *Phys. Rev. A* **91**, 042104 (2015).
- [96] S. Ng, S. Z. Ang, T. A. Wheatley, H. Yonezawa, A. Furusawa, E. H. Huntington, and M. Tsang, *Phys. Rev. A* **93**, 042121 (2016).
- [97] J. Kolodynski and R. Demkowicz-Dobrzanski, *New J. Phys.* **15**, 073043 (2013).
- [98] M. B. Plenio and P. L. Knight, *Rev. Mod. Phys.* **70**, 101 (1998).
- [99] S. Gleyzes, S. Kuhr, C. Guerlin, J. Bernu, S. Deléglise, U. Busk Hoff, M. Brune, J.-M. Raimond, and S. Haroche, *Nature (London)* **446**, 297 (2007).
- [100] J. Piilo, S. Maniscalco, K. Härkönen, and K.-A. Suominen, *Phys. Rev. Lett.* **100**, 180402 (2008).
- [101] Y. Yu, S.-L. Zhu, G. Sun, X. Wen, N. Dong, J. Chen, P. Wu, and S. Han, *Phys. Rev. Lett.* **101**, 157001 (2008).
- [102] A. N. Vamivakas, C.-Y. Lu, C. Matthiesen, Y. Zhao, S. Falt, A. Badolato, and M. Atature, *Nature (London)* **467**, 297 (2010).
- [103] A. Delteil, W. B. Gao, P. Fallahi, J. Miguel-Sanchez, and A. Imamoglu, *Phys. Rev. Lett.* **112**, 116802 (2014).
- [104] P. Campagne-Ibarcq, P. Six, L. Bretheau, A. Sarlette, M. Mirrahimi, P. Rouchon, and B. Huard, *Phys. Rev. X* **6**, 011002 (2016).
- [105] M. Naghiloo, N. Foroozani, D. Tan, A. Jadbabaie, and K. W. Murch, *Nat. Commun.* **7**, 11527 (2016).
- [106] A. G. Kofman, S. Ashhab, and F. Nori, *Phys. Rep.* **520**, 43 (2012).
- [107] J. Dressel, M. Malik, F. M. Miatto, A. N. Jordan, and R. W. Boyd, *Rev. Mod. Phys.* **86**, 307 (2014).
- [108] A. N. Jordan, J. Martínez-Rincón, and J. C. Howell, *Phys. Rev. X* **4**, 011031 (2014).
- [109] C. Ferrie and J. Combes, *Phys. Rev. Lett.* **112**, 040406 (2014).
- [110] R. Schirhagl, K. Chang, M. Loretz, and C. L. Degen, *Annu. Rev. Phys. Chem.* **65**, 83 (2014).
- [111] M. A. Nielsen and I. L. Chuang, *Quantum Computation and Quantum Information* (Cambridge University, Cambridge, 2000).
- [112] S. Pirandola and C. Lupo, *Phys. Rev. Lett.* **118**, 100502 (2017).
- [113] S. Knysh, V. N. Smelyanskiy, and G. A. Durkin, *Phys. Rev. A* **83**, 021804 (2011).
- [114] Y. M. Zhang, X. W. Li, W. Yang, and G. R. Jin, *Phys. Rev. A* **88**, 043832 (2013).
- [115] J. Liu, X. Jing, and X. Wang, *Phys. Rev. A* **88**, 042316 (2013).
- [116] X.-X. Jing, J. Liu, W. Zhong, and X.-G. Wang, *Commun. Theor. Phys.* **61**, 115 (2014).
- [117] J. Dittmann, *J. Phys. A: Math. Gen.* **32**, 2663 (1999).
- [118] W. Zhong, Z. Sun, J. Ma, X. Wang, and F. Nori, *Phys. Rev. A* **87**, 022337 (2013).
- [119] U. von Toussaint, *Rev. Mod. Phys.* **83**, 943 (2011).